Journal of Applied Analysis and Computation
Volume *, Number *, * *, 1–25
Website:http://www.jaac-online.com
DOI:10.11948/***

A CONVERGENT NUMERICAL APPROXIMATION FOR THE COUPLED MAXWELL-LANDAU-LIFSHITZ-GILBERT EQUATIONS WITH INERTIA EFFECTS

Raymond Kitengeso[1,†] and Zhoushun Zheng[1]

Abstract This study aims to analyze the coupled finite element and boundary element (FEM-BEM) solution to the nonlinear system of Maxwell and inertia Landau–Lifshitz–Gilbert equations. An algorithm is proposed to numerically solve the weak form of this problem, which requires solving coupled linear systems per time step. The algorithm is coupled in the sense that it consists of the sequential computation of the magnetic and electric fields in both the interior and boundary domains, and magnetization afterward. Under some mild assumptions on the effective field, the findings show that the algorithm converges towards a weak solution of the Maxwell-Inertia Landau–Lifshitz–Gilbert system. Numerical experiments demonstrate the algorithm's applicability for a theoretical micromagnetic example.

Keywords Maxwell , Landau–Lifshitz–Gilbert , convergence , FEM-BEM

MSC(2010) 35Q61 , 65M12 , 65M38 , 65M60

1. Introduction

Understanding magnetization phenomena in micromagnetics using Landau-Lifshitz-Gilbert (LLG) models is relevant to the development of magnetic sensors, recording, and storage devices [1]. Fascinating challenges arise when developing and implementing numerical solutions to various LLG models as they are highly non-linear partial differential equations (PDEs), have non-convex constraints, and have several equivalent forms [2, 3].

The various formulations of the LLG equation [5, 6, 24] have been used for the numerical investigation of micromagnetics. The common convergent algorithms implemented to solve LLG-based models have either used the finite difference method (FDM) [7, 8] or the finite element method (FEM) [9, 10] for the discretization of the space domain. The inertial LLG equation (ILLG) extended to account for short-time scales magnetization dynamics [9, 11, 12] has also been analyzed. To further account for electromagnetics dynamics, Maxwell equations have been

†The corresponding author.
[1]School of Mathematics and Statistics, Central South University, Changsha, 410083 Hunan, China
[1]The authors were supported by National Natural Science Foundation of China (51974377) and China Scholarship Council (2020GBJ00921).
Email:kitengeso@csu.edu.cn (Raymond Kitengeso), zszheng@csu.edu.cn (Zhoushun Zheng)

coupled with LLG equations in multiple studies [13–15, 24].

This work proposes combining the coupled Maxwell system and inertial LLG (ILLG) equation to investigate the convergence of a system that accounts for ultrafast magnetism and electromagnetics dynamics. The resulting Maxwell-inertia-Landau–Lifshitz–Gilbert (MILLG) equations model the electromagnetic characteristics of a ferromagnetic material. Analysis of the coupled MILLG equations (1.11-1.15) using a combination of the finite elements method (FEM) in the interior domain discretization with the boundary elements method (BEM) on the boundary discretization was carried out. In contrast with a previous study [16], which uses time-dependent boundary integral formulation for external Maxwell reformulation, this work employs a space-dependent approach [17, 18], which reduces the computational complexity of the MILLG system. The numerical scheme uses the backward Euler method for time-stepping discretization. These schemes have been reliable for convergence and stability on complex PDEs where LLG is non-linearly coupled to other non-linear PDE systems, such as in previous seminal studies [14, 16, 19]. We establish convergence of the approximations towards a weak solution of the problem. Various numerical experiments have been performed to demonstrate convergence in time and space.

This paper is organized as follows: Section 1 formally proposes our problem model (1.1-1.7) and reformulates MILLG equations (1.11-1.15). Then, we recollect the notion of a weak solution (Definition 2.1) in Section 2 and define preliminaries for time and space discretization. In Section 3, we propose a numerical algorithm (Algorithm 1) to approximate the discrete weak formulation of the MILLG system. The wide Section 4 is then dedicated to presenting our main convergence result (Theorem 4.1) and its proof. Lastly, we illustrate convergence in space and time with numerical experiments in Section 5.

1.1. Preliminary mathematical notations

In the current study, assume that the interior domain $\Omega \in \mathbb{R}^3$ and denote its boundary by $\partial\Omega = \Gamma$ be a ferromagnetic material that is embedded into a bounded exterior domain $\hat{\Omega} = \mathbb{R}^3 \setminus \Omega$ (with perfectly conducting outer surface $\partial\hat{\Omega} = \hat{\Gamma}$). Furthermore, assume that $\hat{\Omega} \setminus \bar{\Omega}$ is a vacuum and here $\bar{\Omega}$ denotes the closure of Ω, the interior domain $\Omega_T := [0,T] \times \Omega$ and the exterior domain $\hat{\Omega}_T := [0,T] \times \hat{\Omega}$ for magnetization time T. Inside the domain, the aforementioned parameters are the applied current density $\boldsymbol{J} : \Omega \to \mathbb{R}^3$, the electric and magnetic permeability matrices $\epsilon, \mu : \Omega \to \mathbb{R}^{3\times3}$ and ferromagnetic domain conductivity $\sigma : \Omega \to \mathbb{R}^{3\times3}$. The other parameters are α, which denotes damping, and C_e, which represents exchange, are positive constants. Outside the domain, the following material parameters are treated as constant scalars: $\mu = \mu_0$, $\epsilon = \epsilon_0$, $\sigma = 0$.

1.2. MILLG model problem

We can define the full MILLG system as follows: The magnetization field $\boldsymbol{m} : \Omega \to \mathbb{S}^2$, where $\mathbb{S}^2$ is the unit sphere, and electric and magnetic fields $\boldsymbol{E}, \boldsymbol{H} : \Omega \cup \hat{\Omega} \to \mathbb{R}^3$ satisfy the coupled system (1.1-1.7):

For interior domain $[0,T]\times\Omega$

$$\frac{\partial \boldsymbol{m}}{\partial t} = -\boldsymbol{m}\times\boldsymbol{H}_{\text{eff}} + \alpha\boldsymbol{m}\times\frac{\partial \boldsymbol{m}}{\partial t} + \omega\boldsymbol{m}\times\frac{\partial^2\boldsymbol{m}}{\partial t^2}, \quad \text{in } \Omega_T, \tag{1.1}$$

$$\epsilon\frac{\partial \boldsymbol{E}}{\partial t} = (\nabla\times\boldsymbol{H}) - \sigma\boldsymbol{E} - \boldsymbol{J}, \quad \text{in } \Omega_T, \tag{1.2}$$

$$\mu\frac{\partial \boldsymbol{H}}{\partial t} = -(\nabla\times\boldsymbol{E}) - \mu\frac{\partial \boldsymbol{m}}{\partial t}, \quad \text{in } \Omega_T, \tag{1.3}$$

and for exterior domain $[0,T]\times\hat{\Omega}$

$$\epsilon_0\frac{\partial \boldsymbol{E}}{\partial t} = \nabla\times\boldsymbol{H}, \quad \text{in } \hat{\Omega}_T, \tag{1.4}$$

$$\mu_0\frac{\partial \boldsymbol{H}}{\partial t} = -\nabla\times\boldsymbol{E}, \quad \text{in } \hat{\Omega}_T. \tag{1.5}$$

The system is supplemented with initial conditions

$$\begin{aligned} \boldsymbol{m}(0,\boldsymbol{x}) = \boldsymbol{m}^0, \quad \boldsymbol{E}(0,\boldsymbol{x}) = \boldsymbol{E}^0, \quad \boldsymbol{H}(0,\boldsymbol{x}) = \boldsymbol{H}^0 \quad &\text{in } \Omega_T, \\ \boldsymbol{E}(0,\boldsymbol{x}) = 0, \quad \boldsymbol{H}(0,\boldsymbol{x}) = 0 \quad &\text{in } \hat{\Omega}_T, \end{aligned} \tag{1.6}$$

and with the boundary $\Gamma_T := [0,T]\times\Gamma$ condition for magnetization

$$\partial_{\boldsymbol{n}}\boldsymbol{m} = 0 \quad \text{on } \Gamma_T, \tag{1.7}$$

together with jump conditions connecting the two domains

$$\begin{aligned} \gamma_L\boldsymbol{E} &= \hat{\gamma}_L\boldsymbol{E} \quad \text{on } \Gamma, \\ \gamma_M\boldsymbol{H} &= \hat{\gamma}_M\boldsymbol{H} \quad \text{on } \Gamma, \end{aligned} \tag{1.8}$$

where $\boldsymbol{n}$ denotes the outward pointing normal vector, $\hat{\gamma}_M$ and $\hat{\gamma}_L$ are Neumann and tangential traces on Γ respectively. For simplicity, consider some high-order energy contributions by applied and exchange fields [20]. We then have the effective magnetic field $\boldsymbol{H}_{\text{eff}}$ given by

$$\boldsymbol{H}_{\text{eff}}(\boldsymbol{x},t) = C_e\Delta\boldsymbol{m}(t,\boldsymbol{x}) + \boldsymbol{H}(t,\boldsymbol{x}).$$

Here $\boldsymbol{H}$ denotes a given applied field, and $C_e\Delta\boldsymbol{m}$ represents the exchange field, which depends on the energy functional $E(\boldsymbol{m}) = \frac{C_e}{2}\int_\Omega |\Delta\boldsymbol{m}|^2 d\boldsymbol{x}$.

1.3. MILLG model reformulation

In this part, motivated by [17], we transform external domain $\hat{\Omega}$ Maxwell's equations into boundary domain Γ integral equations. We obtain a coupled Maxwell system between internal domain Ω and boundary domain Γ, which, put together with ILLG, form the full MILLG system. Firstly, only take into account Maxwell's equations (1.3-1.5) together with jump conditions (1.8). One can refer to [18] for rigorous requirements of uniqueness, and at the moment, the derivation is done at a conventional level.

Let $\hat{\boldsymbol{E}}(\boldsymbol{x})$ and $\hat{\boldsymbol{H}}(\boldsymbol{x})$ represent space-dependent exterior magnetic and electric fields that satisfy time-harmonic Maxwell equations (1.4) and (1.5) respectively, as in

([18], Section 4.1). Let $\boldsymbol{n}$ be the exterior normal vector on Γ pointing into $\hat{\Omega}$. Recollect equations (1.3-1.5) and define the Neumann and tangential traces operators for the exterior domain by $\hat{\gamma}_L \boldsymbol{a} = \hat{\gamma}_M \boldsymbol{a} \times \boldsymbol{n}$ so that the jump conditions are given by

$$\begin{aligned} \gamma_L \boldsymbol{E} &= \hat{\gamma}_L \hat{\boldsymbol{E}} \quad \text{on } \Gamma, \\ \gamma_M \boldsymbol{H} &= \hat{\gamma}_M \hat{\boldsymbol{H}} \quad \text{on } \Gamma. \end{aligned}$$

From scattering theory [18], for a fixed $\boldsymbol{x}, \boldsymbol{y} \in \mathbb{C}$, one can write Maxwell equations for the electric field and magnetic fields corresponding to the exterior problem as

$$\begin{aligned} \nabla \times \hat{\boldsymbol{E}} &= ik\hat{\boldsymbol{H}} \quad \text{in } \hat{\Omega}, \\ \nabla \times \hat{\boldsymbol{H}} &= -ik\hat{\boldsymbol{E}} \quad \text{in } \hat{\Omega}, \end{aligned} \tag{1.9}$$

where $\hat{\boldsymbol{E}} = \boldsymbol{E}_{inc} + \boldsymbol{E}_{scat}$ and $\hat{\boldsymbol{H}} = \boldsymbol{H}_{inc} + \boldsymbol{H}_{scat}$ and $\boldsymbol{E}_{inc}$ and $\boldsymbol{H}_{inc}$ are incident magnetic and electric fields respectively, $\boldsymbol{E}_{scat}$ and $\boldsymbol{H}_{scat}$ are scattered magnetic and electric fields respectively, and k is the wavenumber. One can write the exterior scattering problem (1.9) as follows, find $\hat{\boldsymbol{E}} = \boldsymbol{E}_{inc} + \boldsymbol{E}_{scat}$ satisfying:

$$\begin{aligned} \nabla \times \left(\nabla \times \hat{\boldsymbol{E}} \right) &= k^2 \hat{\boldsymbol{E}} \quad \text{in } \hat{\Omega}, \\ \hat{\boldsymbol{E}} \times \boldsymbol{n} &= 0 \quad \text{on } \hat{\Gamma}, \\ \lim_{|\boldsymbol{x}| \to \infty} |\boldsymbol{x}| \left(\nabla \times \boldsymbol{E}_{scat} \times \frac{\boldsymbol{x}}{|\boldsymbol{x}|} - \mathrm{i}k\boldsymbol{E}_{\mathrm{s}} \right) &= 0 \quad \text{as } |\boldsymbol{x}| \to \infty. \end{aligned}$$

where $\boldsymbol{H}_{inc} = \boldsymbol{n} \times \boldsymbol{E}_{inc}$, $\hat{\boldsymbol{x}} = \boldsymbol{x}/|\boldsymbol{x}|$, $\phi\gamma_M = -\boldsymbol{E}_{scat} = \boldsymbol{E} - \boldsymbol{E}_{inc}$ and $\psi\gamma_L = -\boldsymbol{H}_{scat} = \boldsymbol{H} - \boldsymbol{H}_{inc}$.
As defined in ([17], Section 4), the exterior Calderon projector is given as, $\hat{\mathcal{C}} = \frac{1}{2}\mathrm{Id} - A$ and it can be written in matrix form as

$$\hat{\mathcal{C}} = \begin{bmatrix} \hat{\gamma}_M \phi & \hat{\gamma}_L \boldsymbol{\phi} \\ \hat{\gamma}_M \psi & \hat{\gamma}_L \boldsymbol{\psi} \end{bmatrix} = \begin{bmatrix} \frac{1}{2}\mathrm{Id} - V & K \\ -K & \frac{1}{2}\mathrm{Id} - V \end{bmatrix}, \tag{1.10}$$

where Id is the identity operator that maps every function to itself, and A is the multitrace boundary operator matrix given by

$$A := \begin{bmatrix} V & K \\ -K & V \end{bmatrix},$$

where V and K are the discretizations of the electric and magnetic boundary operators with the corresponding electric and magnetic potential operators ϕ and, ψ, respectively.
One can directly obtain the electric field integral equation (EFIE), which can be derived from the first line of the exterior Calderon projector 1.10 to obtain $V\pi = \frac{1}{2}\hat{\gamma}_L(\mathrm{Id} + K)\boldsymbol{E}_{inc}$. In addition, the strong form of magnetic field integral equation (MFIE) can be represented directly as EFIE by $(K - \frac{1}{2}\mathrm{Id})\eta = \hat{\gamma}_L \boldsymbol{E}_{inc}$. Here, π represents the Neumann trace of the scattered field, and η represents the tangential trace of the scattered field. A well-conditioned mass matrix B is required to obtain

invertible choices of dual and range spaces in the discretization of $A^2 = \frac{1}{4}\mathrm{Id}$.

$$B\begin{bmatrix}\boldsymbol{\phi}\\ \boldsymbol{\psi}\end{bmatrix} = \frac{1}{2\mu_0}\begin{bmatrix}\hat{\gamma}_L(\mathrm{Id}+K)\boldsymbol{E}_{inc}\\ \hat{\gamma}_L\boldsymbol{E}_{inc}\end{bmatrix} = \frac{1}{2\mu_0}\begin{bmatrix}\hat{\gamma}_L(\mathrm{Id}+K)\boldsymbol{E}_{inc}\\ \hat{\gamma}_M(\mathrm{Id}-V)\boldsymbol{H}_{inc}\end{bmatrix},$$

$$B\begin{bmatrix}\boldsymbol{\phi}\\ \boldsymbol{\psi}\end{bmatrix} = \frac{1}{2}\begin{bmatrix}\mu_0^{-1}\gamma_L\boldsymbol{E}\\ -\gamma_M\boldsymbol{E}\end{bmatrix} = \frac{1}{2}\begin{bmatrix}\mu_0^{-1}\gamma_L\boldsymbol{E}\\ \gamma_L\boldsymbol{H}\end{bmatrix},$$

where $\boldsymbol{E}_{inc}$ can be defined as $\boldsymbol{q}e^{ik\boldsymbol{d}\cdot\boldsymbol{x}}$ with $\boldsymbol{H}_{inc} = \boldsymbol{n}\times\boldsymbol{E}_{inc}$, where $\boldsymbol{d}$ is the direction of the incoming field.
With the Calderon operator together with mass matrix B introduced, we reformulate the coupled MILLG system (1.1) - (1.8) on Ω and its boundary Γ: find functions $\boldsymbol{m}:\Omega\to\mathbb{S}^2$, $\boldsymbol{E},\boldsymbol{H}:\Omega\to\mathbb{R}^3$ and $\boldsymbol{\phi},\boldsymbol{\psi}:\Gamma\to\mathbb{R}^3$ which satisfy (1.11-1.15):

$$\partial_t\boldsymbol{m} = -\boldsymbol{m}\times(C_e\Delta\boldsymbol{m}+\boldsymbol{H}) + \alpha\boldsymbol{m}\times\partial_t\boldsymbol{m} + \omega\boldsymbol{m}\times\partial_t^2\boldsymbol{m}, \quad \text{in } \Omega_T, \tag{1.11}$$

$$\epsilon\partial_t\boldsymbol{E} = (\nabla\times\boldsymbol{H}) - \sigma\boldsymbol{E} - \boldsymbol{J}, \quad \text{in } \Omega_T, \tag{1.12}$$

$$\mu\partial_t\boldsymbol{H} = -(\nabla\times\boldsymbol{E}) - \mu\partial_t\boldsymbol{m}, \quad \text{in } \Omega_T, \tag{1.13}$$

and

$$B\begin{bmatrix}\boldsymbol{\phi}\\ \boldsymbol{\psi}\end{bmatrix} = \frac{1}{2}\begin{bmatrix}\mu_0^{-1}\gamma_L\boldsymbol{E}\\ \gamma_L\boldsymbol{H}\end{bmatrix} \quad \text{on } \Gamma, \tag{1.14}$$

with the boundary $\Gamma_T := [0,T]\times\Gamma$ condition

$$\partial_n\boldsymbol{m} = 0 \quad \text{on } \Gamma_T. \tag{1.15}$$

From now onward, the equivalent reformulated MILLG model (1.11-1.15) will be employed for analysis and investigation.

2. Weak solution to the MILLG system

This section presents the definition and discretization of a weak solution to the MILLG equations (1.11-1.15). Consider some functional spaces and assume some conditions on the initial functions $\boldsymbol{m}^0$, $\boldsymbol{E}^0$, and $\boldsymbol{H}^0$.
The function spaces $\mathbb{H}^1(\Omega,\mathbb{R}^3)$ and $\mathbb{H}(\mathrm{curl};\Omega)$ are defined as follows:

$$\mathbb{H}^1(\Omega,\mathbb{R}^3) = \left\{\boldsymbol{g}\in\mathbb{L}^2(\Omega,\mathbb{R}^3) : \frac{\partial\boldsymbol{g}}{\partial x_i}\in\mathbb{L}^2(\Omega,\mathbb{R}^3) \quad \text{for} \quad i=1,2,3\right\},$$
$$\mathbb{H}(\mathrm{curl};\Omega) = \left\{\boldsymbol{g}\in\mathbb{L}^2(\Omega,\mathbb{R}^3) : \nabla\times\boldsymbol{g}\in\mathbb{L}^2(\Omega,\mathbb{R}^3)\right\}.$$

In this case, for a domain $\Omega\subset\mathbb{R}^3$, $\mathbb{L}^2(\Omega,\mathbb{R}^3)$ is the typical space of Lebesgue squared integrable functions defined on Ω and taking values in $\mathbb{R}^3$. Also, denote

$$\langle\cdot,\cdot\rangle_\Omega := \langle\cdot,\cdot\rangle_{\mathbb{L}^2(\Omega,\mathbb{R}^3)} \quad \text{and} \quad \|\cdot\|_\Omega := \|\cdot\|_{\mathbb{L}^2(\Omega,\mathbb{R}^3)}.$$

To define a weak solution of MILLG equations, assume that the given initial functions $\boldsymbol{m}^0 \in \mathbb{H}^1(\Omega, \mathbb{R}^3)$ and $\boldsymbol{E}^0, \boldsymbol{H}^0 \in \mathbb{H}(\text{curl}; \Omega)$ satisfy

$$\begin{aligned} |\boldsymbol{m}^0| = 1, \quad \text{div}(\boldsymbol{H}^0 + \boldsymbol{m}^0) = \text{div}(\boldsymbol{H}^0) = 0, \quad \text{div}(\boldsymbol{E}^0) = 0 \quad \text{in} \quad \Omega, \\ \text{div}\boldsymbol{J}(\boldsymbol{x}, t) = 0 \quad \text{in} \quad \Omega, \\ (\boldsymbol{H}^0 + \boldsymbol{m}^0) \cdot \boldsymbol{n} = 0 \quad \text{on} \quad \Gamma_T. \end{aligned} \tag{2.1}$$

Since we have reformulated the MILLG model, instead of solving (1.1)-(1.8), it is equivalent to solving (1.11)-(1.15). We can now define a weak solution to the MILLG problem (1.11-1.15).

2.1. Weak solution

Definition 2.1. Let the initial data $(\boldsymbol{m}^0, \boldsymbol{E}^0, \boldsymbol{H}^0)$ satisfy (2.1). Then $\boldsymbol{m}, \boldsymbol{H}, \boldsymbol{E}$ is called a weak solution to MILLG equations (1.11)-(1.15) if, for all $T > 0$, the following hold

1. $\boldsymbol{m} \in \mathbb{H}^1(\Omega_T, \mathbb{R}^3)$ with $|\boldsymbol{m}| = 1$ almost everywhere, $\boldsymbol{m}(0) = \boldsymbol{m}^0$ in the sense of traces and, for all test functions $\zeta \in \mathcal{C}^\infty(\Omega_T)$ and let $\boldsymbol{v} = \partial_t \boldsymbol{m}$ we have

$$\langle \alpha \boldsymbol{v}, \zeta \rangle_{\Omega_T} + \langle \boldsymbol{m} \times \boldsymbol{v}, \zeta \rangle_{\Omega_T} + \langle \omega \partial_t \boldsymbol{v}, \zeta \rangle_{\Omega_T} = -\langle C_e \nabla \boldsymbol{m}, \nabla \zeta \rangle_{\Omega_T} + \langle \boldsymbol{H}, \zeta \rangle_{\Omega_T}. \tag{2.2}$$

2. $\boldsymbol{E}$, $\boldsymbol{H}$, $\partial_t \boldsymbol{E}$, $\partial_t \boldsymbol{H} \in \mathbb{L}^2(\Omega_T, \mathbb{R}^3)$ such that $\nabla \times \boldsymbol{E}$, $\nabla \times \boldsymbol{H} \in \mathbb{H}(\text{curl}; \Omega_T)$ with test functions η_E, η_H and the variables $\phi := \mu_0 \gamma_L \boldsymbol{H}$ and $\psi := -\gamma_L \boldsymbol{E}$ with test functions u_ϕ and u_ψ we have

$$\begin{aligned} \langle \epsilon \partial_t \boldsymbol{E}, \eta_E \rangle_{\Omega_T} &= \langle \nabla \times \boldsymbol{H}, \eta_E \rangle_{\Omega_T} - \langle \sigma \boldsymbol{E} + \boldsymbol{J}, \eta_E \rangle_{\Omega_T}, \\ \langle \mu \partial_t \boldsymbol{H}, \eta_H \rangle_{\Omega_T} &= -\langle \nabla \times \boldsymbol{E}, \eta_H \rangle_{\Omega_T} - \langle \mu \boldsymbol{v}, \eta_H \rangle_{\Omega_T}, \\ \left\langle \begin{pmatrix} u_\phi \\ u_\psi \end{pmatrix}, B \begin{pmatrix} \phi \\ \psi \end{pmatrix} \right\rangle_\Gamma &= \frac{1}{2} \left\langle \begin{pmatrix} u_\phi \\ u_\psi \end{pmatrix}, \begin{pmatrix} \mu_0^{-1} \gamma_L \boldsymbol{E} \\ -\gamma_L \boldsymbol{H} \end{pmatrix} \right\rangle_\Gamma. \end{aligned} \tag{2.3}$$

3. for almost all $t \in (0, T)$, we have bounded energy

$$\|\nabla \boldsymbol{m}\|^2_{\mathbb{L}^2(\Omega_T)} + \|\boldsymbol{v}\|^2_{\mathbb{L}^2(\Omega_T)} + \|\partial_t \boldsymbol{v}\|^2_{\mathbb{L}^2(\Omega_T)} + \|\boldsymbol{H}\|^2_{\mathbb{L}^2(\Omega_T)} + \|\boldsymbol{E}\|^2_{\mathbb{L}^2(\Omega_T)} \leq C,$$

where $C > 0$ is independent of t.

Space and time discretizations for MILLG weak form are defined in Definition 2.1.

2.2. Tangent Plane scheme and time discretization

Let $\mathcal{T}_h$ be a regular tetrahedrization of the polyhedral bounded Lipschitz domain $\Omega \subset \mathbb{R}^3$ into compact tetrahedra mesh with maximum size h, and let a set of vertices and edges be represented by $\mathcal{N}_h := \{\boldsymbol{x}_1, ..., \boldsymbol{x}_N\}$, and $\mathcal{M}_h := \{\boldsymbol{e}_1, ..., \boldsymbol{e}_M\}$ respectively.

To discretize the ILLG equation (2.2), we introduce the $\mathcal{P}^1$-FEM space $\mathcal{S}^1_h \subset \mathbb{H}^1(\Omega, \mathbb{R}^3)$ which is the space of all continuous piecewise linear functions on $\mathcal{T}_h$. A basis for $\mathcal{S}^1_h$ can be chosen to be $\varphi_h \in \mathcal{C}(\bar{\Omega}, \mathbb{R}^3)$, where $\varphi_h(\boldsymbol{x}_m) = \delta_{n,m}$. Here

$\delta_{n,m}$ stands for the Kronecker symbol $\delta_{n,m} = \begin{cases} 1, & \text{if } n = m, \\ 0, & \text{if } n \neq m. \end{cases}$. The interpolation operator from $\mathcal{C}^0(\Omega, \mathbb{R}^3)$ onto $\mathcal{S}_h^1$ is denoted by $\boldsymbol{P}_h$,

$$\begin{aligned} \mathcal{S}_h^1 :=& \{\varphi_h \in \mathcal{C}(\bar{\Omega}, \mathbb{R}^3) : \varphi_{h|K} \in \mathcal{P}^1(K) \quad \forall \quad K \in \mathcal{T}_h\}, \\ \boldsymbol{P}_h(\boldsymbol{u}) :=& \sum_{h=1}^{N} \boldsymbol{u}(\boldsymbol{x}_h)\varphi_h(\boldsymbol{x}) \quad \forall \boldsymbol{u} \in \mathcal{C}^0(\Omega, \mathbb{R}^3). \end{aligned}$$

Since $|\boldsymbol{m}(t, \boldsymbol{x})| = 1$ almost everywhere, define the discrete manifold $\mathcal{Y}_h$ and tangent space $\mathcal{K}_h$ for any magnetization $\boldsymbol{m}_h \in \mathcal{Y}_h$ as

$$\begin{aligned} \mathcal{Y}_h :=& \{\varphi_h \in \mathcal{S}_h^1 || \varphi_h(\boldsymbol{x})| = 1 \quad \forall \quad \boldsymbol{x} \in \mathcal{N}_h\}, \\ \mathcal{K}_h :=& \{\varphi_h \in \mathcal{S}_h^1 : \boldsymbol{m}_h \cdot \varphi_h(\boldsymbol{x}) = 0 \quad \forall \quad \boldsymbol{x} \in \mathcal{N}_h\}. \end{aligned}$$

To discretize Maxwell's equation (2.3) in the interior, we use a Nedelec conforming ansartz space [14]. Let $\{\boldsymbol{\pi}_1, ..., \boldsymbol{\pi}_M\}$ be a basis for lowest order edge elements of Nedelec first family space $\mathcal{X}_h^1 \subset \mathbb{H}(\text{curl}, \Omega)$. We define the following interpolation operator $\boldsymbol{Q}_h$ from $\mathcal{C}^\infty(\Omega)$ onto $\mathcal{X}_h^1$,

$$\begin{aligned} \mathcal{X}_h^1 :=& \{\pi_h \in \mathbb{H}(\text{curl}, \Omega) : \pi_{h|K} \in \mathcal{P}_{skw}^1(K) \quad \forall \quad K \in \mathcal{T}_h\}, \\ \text{where} \quad \mathcal{P}_{skw}^1(K) =& \{v : K \to \mathbb{R}^3, v(x) = a + Bx : a \in \mathbb{R}^3, B \in \mathbb{R}^{3\times 3}, B^T = -B\}, \\ \boldsymbol{Q}_h(\boldsymbol{w}) =& \sum_{q=1}^{M} \left(\int_{e_q} \boldsymbol{w} \cdot \nu_q ds \right) \pi_q \quad \forall \boldsymbol{w} \in \mathcal{C}^\infty(\Omega, \mathbb{R}^3). \end{aligned}$$

With the finite element spaces defined above, now define the approximation scheme. For time discretization, use a constant time step size $\tau := \frac{T}{N}$ for a fixed positive integer $N \in \mathbb{N}$ with time steps $0 = t_0, ..., t_n = T$, $t_j = \tau j$. For $j = 1, 2, ..., N$, the functions $\boldsymbol{m}(t_j, \cdot)$, $\boldsymbol{E}(t_j, \cdot)$ and $\boldsymbol{H}(t_j, \cdot)$ are approximated by $\boldsymbol{m}_h^j \in \mathcal{S}_h^1$ and $\boldsymbol{E}_h^j, \boldsymbol{H}_h^j \in \mathcal{X}_h^1$ respectively.
Noting from (1.1) that $\partial_t \boldsymbol{m} \cdot \boldsymbol{m} = 0$ and recall φ_h is a basis of $\mathcal{S}_h^1$, we find $\boldsymbol{v}^{j+1}$ in the space $\mathbb{V}_h^j$ and $|\boldsymbol{m}^{j+1}| = 1$ condition defined by

$$\begin{aligned} \mathbb{V}_h^j :=& \{\boldsymbol{v} \in \mathcal{S}_h^1 | \boldsymbol{v}(\boldsymbol{x}_n) \cdot \boldsymbol{m}_h^j(\boldsymbol{x}_n) = 0, n = 1, ..., N\}, \\ |\boldsymbol{m}_h^{j+1}| :=& \sum_{n=1}^{N} \frac{\boldsymbol{m}_h^j(\boldsymbol{x}_n) + \tau \boldsymbol{v}_h^{j+1}(\boldsymbol{x}_n)}{|\boldsymbol{m}_h^j(\boldsymbol{x}_n) + \tau \boldsymbol{v}_h^{j+1}(\boldsymbol{x}_n)|} \varphi_h. \end{aligned}$$

3. FEM-BEM Algorithm

In this section, we implement FEM for the ILLG part in the interior domain and coupling of FEM-BEM for the Maxwell part in the interior and boundary domains. We approximate the solution of the MILLG system (1.11) to (1.15) by the following algorithm, based on the weak formulation Definition 2.1:

Algorithm 1: FEM-BEM Algorithm

1. **Input**: discretized initial data $\boldsymbol{m}_h^0, \boldsymbol{E}_h^0, \boldsymbol{H}_h^0, \boldsymbol{\phi}_h^0, \boldsymbol{\psi}_h^0$ and the implicity parameter $\theta \in [0,1]$.
2. **for** $j \to j+1, j \in \mathbb{N}$, $0 \le j \le N-1$. Compute the following:

a. Given $\boldsymbol{m}_h^j$, $\boldsymbol{H}_h^j$, compute $\boldsymbol{v}_h^{j+1} \in \mathcal{K}_h$ by solving the bilinear form of the ILLG equation (2.2) discretized below for all $\zeta_h \in \mathcal{K}_h$

$$\begin{aligned} \langle \alpha \boldsymbol{v}_h^j, \zeta_h\rangle_{\Omega_T} + \langle \boldsymbol{v}_h^j \times \boldsymbol{m}_h^j, \zeta_h\rangle_{\Omega_T} + \langle \omega(\boldsymbol{v}_h^{j+1} - \boldsymbol{v}_h^j)/\tau, \zeta_h\rangle_{\Omega_T} = \\ -\langle C_e \nabla(\boldsymbol{m}_h^j + \theta\tau \boldsymbol{v}_h^j), \nabla\zeta_h\rangle_{\Omega_T} + \langle \boldsymbol{H}_h^j, \zeta_h\rangle_{\Omega_T}, \end{aligned} \tag{3.1}$$

b. Compute $\boldsymbol{E}_h^{j+1}$, $\boldsymbol{H}_h^{j+1} \in \mathcal{X}_h^1$ and $\boldsymbol{\phi}_h^{j+1} \in \gamma_L(\mathcal{X}_h^1)$, $\boldsymbol{\psi}_h^{j+1} \in \gamma_L(\mathcal{X}_h^1)$ by solving in block form the Maxwell equation (2.3) discretized below for all $\eta_{Eh}, \eta_{Hh} \in \mathcal{X}_h^1$ and $u_\phi \in \gamma_L(\mathcal{X}_h^1), u_\psi \in \gamma_L(\mathcal{X}_h^1)$

$$\begin{aligned} \langle (\epsilon/\tau + \sigma)\, \boldsymbol{E}_h^{j+1}, \eta_{Eh}\rangle_{\Omega_T} - \langle \nabla \times \boldsymbol{H}_h^{j+1}, \eta_{Eh}\rangle_{\Omega_T} = \\ \langle (\epsilon/\tau)\boldsymbol{E}_h^j, \eta_{Eh}\rangle_{\Omega_T} - \langle \boldsymbol{J}_h^{j+1}, \eta_{Eh}\rangle_{\Omega_T}, \\ \langle (\mu/\tau)\boldsymbol{H}_h^{j+1}, \eta_{Hh}\rangle_{\Omega_T} + \langle \nabla \times \boldsymbol{E}_h^{j+1}, \eta_{Hh}\rangle_{\Omega_T} = \\ \langle (\mu/\tau)\boldsymbol{H}_h^j, \eta_{Hh}\rangle_{\Omega_T} - \langle \mu \boldsymbol{v}_h^j, \eta_{Hh}\rangle_{\Omega_T}, \\ \left\langle \begin{pmatrix} u_\phi \\ u_\psi \end{pmatrix}, B \begin{pmatrix} \phi_h^{j+1} \\ \psi_h^{j+1} \end{pmatrix} \right\rangle_\Gamma = \frac{1}{2} \left\langle \begin{pmatrix} u_\phi \\ u_\psi \end{pmatrix}, \begin{pmatrix} \mu_0^{-1}\gamma_L \boldsymbol{E}_h^{j+1} \\ -\gamma_L \boldsymbol{H}_h^{j+1} \end{pmatrix} \right\rangle_\Gamma. \end{aligned} \tag{3.2}$$

Maxwell equations can be written in block form as:

$$\begin{bmatrix} B[0,0] & B[0,1] & B[0,2] & B[0,3] \\ B[1,0] & B[1,1] & B[1,2] & B[1,3] \\ B[2,0] & B[2,1] & B[2,2] & B[2,3] \\ B[3,0] & B[3,1] & B[3,2] & B[3,3] \end{bmatrix} \begin{bmatrix} \boldsymbol{E}_h^{i+1} \\ \boldsymbol{H}_h^{i+1} \\ \phi_h^{i+1} \\ \psi_h^{i+1} \end{bmatrix} = \begin{bmatrix} Y[0] \\ Y[1] \\ Y[2] \\ Y[3] \end{bmatrix}.$$

c. We update and normalize by computing $\boldsymbol{m}_h^{j+1}$ for all nodes $x \in \mathcal{N}_h$

$$\begin{aligned} \boldsymbol{m}_h^{j+1}(x) :=& \frac{\boldsymbol{m}_h^j(x) + \tau \boldsymbol{v}_h^j(x)}{|\boldsymbol{m}_h^j(x) + \tau \boldsymbol{v}_h^j(x)|}, \\ \boldsymbol{v}_h^{j+1}(x) :=& \boldsymbol{v}_h^{j+1}(x) + \tau \boldsymbol{v}_h^j(x). \end{aligned} \tag{3.3}$$

3. **Return** to step 2(a) if $j < N$.
4. **Stop** if $j = N$.
5. **Output**: the sequence of approximations $\boldsymbol{m}_h^{j+1}$, $\boldsymbol{E}_h^{i+1}$, $\boldsymbol{H}_h^{i+1}$, $\boldsymbol{\phi}_h^{i+1}$, $\boldsymbol{\psi}_h^{i+1}$.

For tangent plane scheme the implicit parameter θ and $\boldsymbol{R} \in \{\boldsymbol{v}, \boldsymbol{E}, \boldsymbol{H}, \phi, \psi\}$, the

second order discrete-time derivative takes the form

$$\begin{aligned} \partial_t \boldsymbol{R}^{j+1} &= \frac{\boldsymbol{R}^{j+1} - \boldsymbol{R}^j}{\tau}, \\ \boldsymbol{m}_h^{j+1} &= \boldsymbol{m}_h^j + \theta\tau \boldsymbol{v}_h^{j+1}. \end{aligned} \tag{3.4}$$

The parameter θ can be arbitrarily selected in $[0,1]$. The method is explicit when $\theta = 0$ and fully implicit when $\theta = 1$.

Remark 3.1. Here, we use a first-order implicit scheme for the computational stability and efficiency of the coupled system. Meanwhile, discrete energy laws of LLG can be extended to ILLG [9]. Using the same approach, we can design second-order A-stable schemes [26]. However, high-order schemes greater than 2 cannot be A-stable [19].

Assume that the spatial meshes are uniformly shaped, regular, and satisfy the angle condition.

Lemma 3.1. *It holds*

$$\int_\Omega \nabla\varphi_i \cdot \varphi_j d\boldsymbol{x} \le 0 \quad \forall \quad i,j \in \{1,2,...,N\} \quad \text{with} \quad i \ne j.$$

Recall from Section 2.2, that φ_h is a basis of $\mathcal{S}_h^1$. The condition is satisfied if all dihedral angles of the tetrahedral meshes $\mathcal{T}_h$ are smaller than or equal to $\pi/2$; see [21]. Then for all $\boldsymbol{u} \in \mathcal{S}_h^1$ satisfying $|\boldsymbol{u}(\boldsymbol{x}_k)| \ge 1, k = 1,2,...,N$, there holds

$$\int_\Omega \nabla \mathbb{T}_h \left| \frac{\boldsymbol{u}}{|\boldsymbol{u}|} \right|^2 d\boldsymbol{x} \le \int_\Omega |\nabla \boldsymbol{u}|^2 d\boldsymbol{x}.$$

Remark 3.2. The angle condition ensures boundedness of the normalization step in Algorithm 1

$$\|\nabla \boldsymbol{m}_h^{j+1}\|_\Omega \le \|\nabla(\boldsymbol{m}_h^j + \tau \boldsymbol{v}_h^j)\|_\Omega. \tag{3.5}$$

Lemma 3.2. *The trace operators $\gamma_L, \hat{\gamma}_L : \mathbb{H}(\mathrm{curl}; \Omega \cup \hat{\Omega}) \to \mathcal{H}_\Gamma$ and $\gamma_M, \hat{\gamma}_M : \mathbb{H}(\mathrm{curl}^2; \Omega \cup \hat{\Omega}) \to \mathcal{H}_\Gamma$ are continuous and surjective, see ([17], Theorem 1).*

We collected from ([17], Section 3) the tangential trace space, $\mathcal{H}_x^{1/2}(\Gamma)$ and its dual space $\mathcal{H}_x^{-1/2}(\Gamma)$ with respect to antisymmetric product $\langle \boldsymbol{a}, \boldsymbol{b} \rangle := \int_\Gamma \boldsymbol{a} \cdot (\boldsymbol{n} \times \boldsymbol{b})$ for $\boldsymbol{a}, \boldsymbol{b} \in \mathbb{L}_L^2$. Here $\mathcal{H}_x^{1/2}(\Gamma) := \gamma_L(\mathbb{H}^1(\Omega))$. The trace space can be defined as $\mathcal{H}_\Gamma := \mathcal{H}_x^{-1/2}(\mathrm{div}_\Gamma, \Gamma)$, where div_Γ denotes the scalar surface divergence.
The discrete solutions $\{\boldsymbol{m}_h^{j+1}, \boldsymbol{E}^{i+1}, \boldsymbol{H}^{i+1}, \boldsymbol{\phi}^{i+1}, \boldsymbol{\psi}^{i+1}\}$ constructed in Algorithm 1 are interpolated in time in the following definition.

Definition 3.1. For each $t \in [0,T]$, let $j \in \{0,...,N\}$ be such that $t \in [t_j, t_{j+1}]$. We define for $t \in [0,T]$, recall [24] we have $t_j = \tau j$, $\boldsymbol{R} \in \{\boldsymbol{m}, \boldsymbol{v}, \boldsymbol{E}, \boldsymbol{H}, \phi, \psi\}$ and

$\boldsymbol{x} \in \Omega$

$$
\begin{aligned}
\boldsymbol{R}_{h,\tau}(t,\boldsymbol{x}) =& \frac{t-t_j}{\tau}\boldsymbol{R}_h^{j+1}(\boldsymbol{x}) + \frac{t_{j+1}-t}{\tau}\boldsymbol{R}_h^{j}(\boldsymbol{x}),\\
\boldsymbol{R}_{h,\tau}^{-}(t,\boldsymbol{x}) =& \boldsymbol{R}_h^{j}(\boldsymbol{x}),\\
\boldsymbol{v}_{h,\tau}(t,\boldsymbol{x}) =& \partial_t \boldsymbol{m}_{h,\tau}(t,\boldsymbol{x}),\\
\phi_{t,\tau} = \gamma_L \boldsymbol{E}_{h,\tau}(t,\boldsymbol{x}) \quad &\text{and} \quad \phi_{t,\tau}^{-} = \gamma_L \boldsymbol{E}_h^{j}(\boldsymbol{x}),\\
\psi_{t,\tau} = \gamma_L \boldsymbol{H}_{h,\tau}(t,\boldsymbol{x}) \quad &\text{and} \quad \psi_{t,\tau}^{-} = \gamma_L \boldsymbol{H}_h^{j}(\boldsymbol{x}),
\end{aligned}
$$

4. Main result and convergence analysis

In this section, we seek to show that Algorithm 1 defines a convergent scheme.

4.1. Main result

Theorem 4.1. *Let $(\boldsymbol{m}_{h,\tau}, \boldsymbol{E}_{h,\tau}, \boldsymbol{H}_{h,\tau}, \boldsymbol{\phi}_{h,\tau}, \boldsymbol{\psi}_{h,\tau})$ be the approximations obtained by Algorithm 1 for $\theta \in \left(\frac{1}{2}, 1\right]$. Under condition (3.5), for any $(\tau, h) \to (0,0)$ there exists a subsequence of $(\boldsymbol{m}_{h,\tau}, \boldsymbol{E}_{h,\tau}, \boldsymbol{H}_{h,\tau}, \boldsymbol{\phi}_{h,\tau}, \boldsymbol{\psi}_{h,\tau})$ that converges weakly in $\mathbb{H}^1(\Omega_T) \times \mathbb{L}^2(\Omega_T)^2 \times \mathbb{L}^2(\mathcal{H}_\Gamma)^2$ to a weak solution $(\boldsymbol{m}, \boldsymbol{E}, \boldsymbol{H}, \boldsymbol{\phi}, \boldsymbol{\psi})$ of MILLG. In particular, each accumulation point of $(\boldsymbol{m}_{h,\tau}, \boldsymbol{E}_{h,\tau}, \boldsymbol{H}_{h,\tau}, \boldsymbol{\phi}_{h,\tau}, \boldsymbol{\psi}_{h,\tau})$ is a weak solution of MILLG in the sense of Definition 2.1.*

The three-step proof proceeds to show that discrete quantities and energies are bounded. Thereafter, we established the existence of weakly convergent subsequences, and their limits are identified as weak solutions of MILLG.

4.2. Analysis of Algorithm

The lemma shows that the algorithm is indeed bounded and admits unique solutions in each iterative loop step.

Lemma 4.1. *Algorithm 1 is well-defined in the sense that, for every $j \geq 0$, there exists unique approximations $\boldsymbol{R}^{j+1}$ that satisfy equations (3.1)-(3.2).*

Proof. . For tangent plane scheme equation (3.1), by the Lax-milgram Theorem, for each $j > 0$ there exists a unique solution $(\boldsymbol{m}_h^{j+1}, \boldsymbol{H}_h^{j+1}) \in \mathcal{K}_h^j \times \mathcal{X}_h^1$

Since $|\boldsymbol{m}_h^j(\boldsymbol{x}_n)| = 1$ and $|\boldsymbol{v}_h^{j+1}(\boldsymbol{x}_n) \cdot \boldsymbol{m}_h^j(\boldsymbol{x}_n)| = 0$ for all $n = 1, ..., N$, there holds $|\boldsymbol{m}_h^j(\boldsymbol{x}_n) + \tau \boldsymbol{v}_h^{j+1}(\boldsymbol{x}_n)| \geq 1$. Therefore, the algorithm is well-defined. There also holds $|\boldsymbol{m}_h^{j+1}(\boldsymbol{x}_n)| = 1$ for $n = 1, ..., N$.

For the Maxwell case (3.2), we define the bilinear form $a(\cdot,\cdot)$ and linear functional

$L^j(\cdot)$ on $\mathcal{X}_h^1 \times \mathcal{X}_h^1 \times \gamma_L(\mathcal{X}_h^1) \times \gamma_L(\mathcal{X}_h^1)$ by

$$
\begin{aligned}
a((\Phi,\Psi,\Theta,\Upsilon),(\phi,\psi,\theta,\nu)) &= \langle(\epsilon/\tau+\sigma)\,\Phi,\phi\rangle_{\Omega_T} - \langle\nabla\times\Psi,\psi\rangle_{\Omega_T} + \\
&\langle(\mu/\tau)\Psi,\psi\rangle_{\Omega_T} + \langle\nabla\times\Phi,\phi\rangle_{\Omega_T} + \left\langle \begin{pmatrix}\theta\\ \nu\end{pmatrix}, B_0 \begin{pmatrix}\Theta\\ \Upsilon\end{pmatrix}\right\rangle_{\Gamma}, \\
L^j(\phi,\psi,\theta,\nu) &= \langle(\epsilon/\tau)\boldsymbol{E}^i,\phi\rangle_{\Omega_T} - \langle\boldsymbol{J}^{i+1},\phi\rangle_{\Omega_T} + \langle(\mu/\tau)\boldsymbol{H}^i,\psi\rangle_{\Omega_T} - \\
&\langle\boldsymbol{v}^i,\psi\rangle_{\Omega_T} + \frac{1}{2}\left\langle \begin{pmatrix}\theta\\ \nu\end{pmatrix}, \sum_{k=1}^{j} B_{j+1-k} \begin{pmatrix}\phi_h^k\\ \psi_h^k\end{pmatrix}\right\rangle_{\Gamma}.
\end{aligned}
$$

Equations (3.1)-(3.2) is equivalent to

$$
\begin{aligned}
a((\Phi,\Psi,\Theta,\Upsilon),(\phi,\psi,\theta,\nu)) &= L^j(\phi,\psi,\theta,\nu), \\
\text{for all}\quad (\phi,\psi,\theta,\nu) &\in (\mathcal{X}_h^1 \times \mathcal{X}_h^1 \times \gamma_L(\mathcal{X}_h^1) \times \gamma_L(\mathcal{X}_h^1))
\end{aligned}
$$

Strictness of $a(\cdot,\cdot)$ on $(\mathcal{X}_h^1 \times \mathcal{X}_h^1 \times \gamma_L(\mathcal{X}_h^1) \times \gamma_L(\mathcal{X}_h^1))$ implies the statement of the Lemma 4.1 and since the trace variants $\gamma_L : \mathbb{H}(\mathrm{curl},\Omega) \to \mathcal{H}_\Gamma$ are bounded [14], we have

$$
\begin{aligned}
a((\Phi,\Psi,\Theta,\Upsilon),(\phi,\psi,\theta,\nu)) &= \langle(\epsilon/\tau+\sigma)\,\Phi,\Phi\rangle_{\Omega_T} + \langle(\mu/\tau)\Psi,\Psi\rangle_{\Omega_T} + \\
&\left\langle \begin{pmatrix}\Theta\\ \Upsilon\end{pmatrix}, B_0 \begin{pmatrix}\Theta\\ \Upsilon\end{pmatrix}\right\rangle_{\Gamma} \\
&\geq C(\tau,\mu,\epsilon,\sigma)(\|\Phi\|_{\Omega_T}^2 + \|\Psi\|_{\Omega_T}^2 + \|\Theta\|_{\mathcal{H}_\Gamma}^2 + \|\Upsilon\|_{\mathcal{H}_\Gamma}^2) > 0,
\end{aligned}
$$

and we conclude the proof. □

Remark 4.1. In this work, we use scalar and constant material parameters $\epsilon, \mu \in \mathbb{R}_+$, but hold with similar arguments for symmetric, coercive, and bounded material tensors $\epsilon, \mu : \Omega_T \to \mathbb{R}^{3\times3}$ and bounded, positive $\sigma : \Omega_T \to \mathbb{R}^{3\times3}$.

The next lemma provides a bound in the $\mathbb{L}^2$-norm for the discrete solutions.

Lemma 4.2. *The sequence* $\{\boldsymbol{m}_h^{j+1}, \boldsymbol{E}^{i+1}, \boldsymbol{H}^{i+1}, \boldsymbol{\phi}^{i+1}, \boldsymbol{\psi}^{i+1}\}$ *produced by Algorithm 1 satisfies*

$$\mathcal{E}^{j-1} \leq C + c\tau \textstyle\sum_{i=1}^{j} \mathcal{E}^{j-2}$$

where

$$\mathcal{E}^{j-1} = \frac{\epsilon}{2}\|\boldsymbol{E}_h^{j-1}\|_{\Omega_T}^2 + \frac{\mu}{2}\|\boldsymbol{H}_h^{j-1}\|_{\Omega_T}^2 + \frac{\tau\omega\mu}{2}\|\boldsymbol{v}_h^{j-1}\|_{\Omega_T}^2 + \frac{\mu C_e}{2}\|\nabla\boldsymbol{m}_h^{j-1}\|_{\Omega_T}^2.$$

$$
\begin{aligned}
C \geq \frac{\epsilon}{2}\left(\sum_{k=1}^{i}\|\boldsymbol{E}_h^{k+1}-\boldsymbol{E}_h^{k}\|_{\Omega_T}^2\right)+\tau\sigma\sum_{k=1}^{i}\|\boldsymbol{E}_h^{k}\|_{\Omega_T}^2+\\
\frac{\mu}{2}\left(\sum_{k=1}^{i}\|\boldsymbol{H}_h^{k+1}-\boldsymbol{H}_h^{k}\|_{\Omega_T}^2\right)+\frac{\mu C_e}{2}\|\nabla\boldsymbol{m}_h^{j+1}\|_{\Omega_T}^2+\\
\tau\alpha\mu\sum_{k=1}^{j}\|\boldsymbol{v}_h^{k}\|_{\Omega_T}^2+\frac{\tau\omega\mu}{2}\left(\sum_{k=1}^{j}\|\boldsymbol{v}_h^{k+1}-\boldsymbol{v}_h^{k}\|_{\Omega_T}^2\right)-\\
\mu C_e\tau^2\left(\frac{1}{2}-\theta\right)\sum_{k=1}^{j}\|\nabla\boldsymbol{v}_h^{k}\|_{\Omega_T}^2+\tau\sum_{k=1}^{j}\left\langle\begin{pmatrix}\phi^k\\ \psi^k\end{pmatrix},B\begin{pmatrix}\phi^{k+1}\\ \psi^{k+1}\end{pmatrix}\right\rangle_{\Gamma}.
\end{aligned}
$$

Proof. Choosing $\boldsymbol{v}_h^j=\zeta_h\in\mathcal{K}_h$ in (3.1) and $\{\boldsymbol{E}^i=\eta_E,\boldsymbol{H}^i=\eta_H,u_\phi=\phi^j,u_\psi=\psi^j\}\in\mathcal{X}_h$ in (3.2), one can obtain

$$
\begin{aligned}
\langle\alpha\boldsymbol{v}_h^j,\boldsymbol{v}_h^j\rangle_{\Omega_T}+\langle\boldsymbol{v}_h^j\times\boldsymbol{m}_h^j,\boldsymbol{v}_h^j\rangle_{\Omega_T}+\langle\omega(\boldsymbol{v}_h^{j+1}-\boldsymbol{v}_h^j)/\tau,\boldsymbol{v}_h^j\rangle_{\Omega_T}=\\
-\langle C_e\nabla(\boldsymbol{m}_h^j+\theta\tau\boldsymbol{v}_h^j),\nabla\boldsymbol{v}_h^j\rangle_{\Omega_T}+\langle\boldsymbol{H}_h^j,\boldsymbol{v}_h^j\rangle_{\Omega_T},
\end{aligned}
\tag{4.1}
$$

$$
\begin{aligned}
\langle(\epsilon/\tau+\sigma)\,\boldsymbol{E}^{i+1},\boldsymbol{E}^i\rangle_{\Omega_T}-\langle\nabla\times\boldsymbol{H}^{i+1},\boldsymbol{E}^i\rangle_{\Omega_T}=\\
\langle(\epsilon/\tau)\boldsymbol{E}^i,\boldsymbol{E}^i\rangle_{\Omega_T}-\langle\boldsymbol{J}^{i+1},\boldsymbol{E}^i\rangle_{\Omega_T},\\
\langle(\mu/\tau)\boldsymbol{H}^{i+1},\boldsymbol{H}^i\rangle_{\Omega_T}+\langle\nabla\times\boldsymbol{E}^{i+1},\boldsymbol{H}^i\rangle_{\Omega_T}=\\
\langle(\mu/\tau)\boldsymbol{H}^i,\boldsymbol{H}^i\rangle_{\Omega_T}-\langle\mu\boldsymbol{v}^i,\boldsymbol{H}^i\rangle_{\Omega_T},\\
\left\langle\begin{pmatrix}\phi^j\\ \psi^j\end{pmatrix},B\begin{pmatrix}\phi^{j+1}\\ \psi^{j+1}\end{pmatrix}\right\rangle_{\Gamma}=\frac{1}{2}\left\langle\begin{pmatrix}\phi^j\\ \psi^j\end{pmatrix},\begin{pmatrix}\mu_0^{-1}\gamma_L\boldsymbol{E}^{j+1}\\ -\gamma_L\boldsymbol{H}^{j+1}\end{pmatrix}\right\rangle_{\Gamma}.
\end{aligned}
\tag{4.2}
$$

Since the angle condition (3.5) is satisfied, we can rewrite equation (4.1) using the following

$$
\begin{aligned}
\|\nabla\boldsymbol{m}_h^{j+1}\|_{\Omega}\leq\|\nabla(\boldsymbol{m}_h^j+\tau\boldsymbol{v}_h^j)\|_{\Omega},\\
\|\nabla\boldsymbol{m}_h^{j+1}\|_{\Omega}^2\leq\|\nabla\boldsymbol{m}_h^j\|_{\Omega}^2+2\tau\langle\nabla\boldsymbol{m}_h^j,\nabla\boldsymbol{v}_h^j\rangle_{\Omega}+\tau^2\|\nabla\boldsymbol{v}_h^j\|_{\Omega}^2.
\end{aligned}
$$

Applying Abel's summation by parts for $\boldsymbol{R}^{i+1}\in\mathbb{R}^3$ to equation (4.1) and (4.2), for $k\leq j\leq i$ it holds that

$$
\sum_{k=1}^{j}\langle(\boldsymbol{R}^{k+1}-\boldsymbol{R}^k),\boldsymbol{R}^k\rangle=\frac{1}{2}\sum_{k=1}^{j}\|\boldsymbol{R}^{k+1}-\boldsymbol{R}^k\|^2+\frac{1}{2}\|\boldsymbol{R}^{j-1}\|^2-\frac{1}{2}\|\boldsymbol{R}^0\|^2.
$$

We rewrite equation (4.1) multiplying by $\tau\mu$ and summing up (4.2) for $k,i,j\in\mathbb{N}$ and we have

$$
\begin{aligned}
\tau\alpha\mu\sum_{k=1}^{j}\|\boldsymbol{v}_h^k\|_{\Omega_T}^2+\frac{\tau\omega\mu}{2}\left(\sum_{k=1}^{j}\|\boldsymbol{v}_h^{k+1}-\boldsymbol{v}_h^k\|_{\Omega_T}^2+\|\boldsymbol{v}_h^{j-1}\|_{\Omega_T}^2-\|\boldsymbol{v}_h^0\|_{\Omega_T}^2\right)\leq\\
-\frac{\mu C_e}{2}\|\nabla\boldsymbol{m}_h^{j+1}\|_{\Omega_T}^2-\frac{\mu C_e}{2}\|\nabla\boldsymbol{m}_h^0\|_{\Omega_T}^2+\\
\mu C_e\tau^2\left(\frac{1}{2}-\theta\right)\sum_{k=1}^{j}\|\nabla\boldsymbol{v}_h^k\|_{\Omega_T}^2+\tau\mu\sum_{k=1}^{j}\langle\boldsymbol{H}_h^k,\boldsymbol{v}_h^k\rangle_{\Omega_T},
\end{aligned}
\tag{4.3}
$$

$$\begin{aligned}
&\frac{\epsilon}{2}\left(\sum_{k=1}^{i}\|\boldsymbol{E}_h^{k+1}-\boldsymbol{E}_h^{k}\|_{\Omega_T}^2+\|\boldsymbol{E}_h^{j-1}\|_{\Omega_T}^2-\|\boldsymbol{E}_h^{0}\|_{\Omega_T}^2\right)+\\
&\frac{\mu}{2}\left(\sum_{k=1}^{i}\|\boldsymbol{H}_h^{k+1}-\boldsymbol{H}_h^{k}\|_{\Omega_T}^2+\|\boldsymbol{H}_h^{j-1}\|_{\Omega_T}^2-\|\boldsymbol{H}_h^{0}\|_{\Omega_T}^2\right)+\\
&\tau\sum_{k=1}^{i}\left\langle\begin{pmatrix}\phi^k\\ \psi^k\end{pmatrix},B\begin{pmatrix}\phi^{k+1}\\ \psi^{k+1}\end{pmatrix}\right\rangle_{\Gamma}\leq\tau\sigma\sum_{k=1}^{i}\|\boldsymbol{E}_h^{k}\|_{\Omega_T}^2-\\
&\tau\mu\sum_{k=1}^{i}\langle\boldsymbol{v}_h^{k},\boldsymbol{H}_h^{k}\rangle_{\Omega_T}-\tau\sum_{k=1}^{j}\langle\boldsymbol{J}_h^{k+1},\boldsymbol{E}_h^{k}\rangle_{\Omega_T}.
\end{aligned}\tag{4.4}$$

Adding equations (4.3) and (4.4) we obtain

$$\begin{aligned}
&\frac{\epsilon}{2}\left(\sum_{k=1}^{i}\|\boldsymbol{E}_h^{k+1}-\boldsymbol{E}_h^{k}\|_{\Omega_T}^2+\|\boldsymbol{E}_h^{j-1}\|_{\Omega_T}^2\right)+\tau\sigma\sum_{k=1}^{i}\|\boldsymbol{E}_h^{k}\|_{\Omega_T}^2+\\
&\frac{\mu}{2}\left(\sum_{k=1}^{i}\|\boldsymbol{H}_h^{k+1}-\boldsymbol{H}_h^{k}\|_{\Omega_T}^2+\|\boldsymbol{H}_h^{j-1}\|_{\Omega_T}^2\right)+\frac{\mu C_e}{2}\|\nabla\boldsymbol{m}_h^{j+1}\|_{\Omega_T}^2+\\
&\tau\alpha\mu\sum_{k=1}^{j}\|\boldsymbol{v}_h^{k}\|_{\Omega_T}^2+\frac{\tau\omega\mu}{2}\left(\sum_{k=1}^{j}\|\boldsymbol{v}_h^{k+1}-\boldsymbol{v}_h^{k}\|_{\Omega_T}^2+\|\boldsymbol{v}_h^{j-1}\|_{\Omega_T}^2\right)-\\
&\mu C_e\tau^2\left(\frac{1}{2}-\theta\right)\sum_{k=1}^{j}\|\nabla\boldsymbol{v}_h^{k}\|_{\Omega_T}^2+\tau\sum_{k=1}^{j}\left\langle\begin{pmatrix}\phi^k\\ \psi^k\end{pmatrix},B\begin{pmatrix}\phi^{k+1}\\ \psi^{k+1}\end{pmatrix}\right\rangle_{\Gamma}\leq\\
&\tau\mu\sum_{k=1}^{j}\langle\boldsymbol{H}_h^{k}-\boldsymbol{H}_h^{k+1},\boldsymbol{v}_h^{k}\rangle_{\Omega_T}-\tau\sum_{k=1}^{j}\langle\boldsymbol{J}_h^{k+1},\boldsymbol{E}_h^{k}\rangle_{\Omega_T}+\\
&\frac{\epsilon}{2}\|\boldsymbol{E}_h^{0}\|_{\Omega_T}^2+\frac{\mu}{2}\|\boldsymbol{H}_h^{0}\|_{\Omega_T}^2+\frac{\tau\omega\mu}{2}\|\boldsymbol{v}_h^{0}\|_{\Omega_T}^2+\frac{\mu C_e}{2}\|\nabla\boldsymbol{m}_h^{0}\|_{\Omega_T}^2.
\end{aligned}\tag{4.5}$$

As the ferromagnetic domain may not be conductive ($\sigma = 0$), the right-hand side (4.5) can be bounded with Cauchy-Schwarz for arbitrary $\delta_1, \delta_2 > 0$ such that

$$\begin{aligned}
&\tau\mu\sum_{k=1}^{j}\langle\boldsymbol{H}_h^{k}-\boldsymbol{H}_h^{k+1},\boldsymbol{v}_h^{k}\rangle_{\Omega_T}-\tau\sum_{k=1}^{j}\langle\boldsymbol{J}_h^{k+1},\boldsymbol{E}_h^{k}\rangle_{\Omega_T}\leq\\
&\sum_{k=1}^{j}\frac{\tau}{2\delta_1}\|\boldsymbol{J}_h^{k+1}\|_{\Omega_T}^2+\sum_{k=1}^{j}\tau\delta_1\|\boldsymbol{E}_h^{k}\|_{\Omega_T}^2+\sum_{k=1}^{j}\frac{\tau\mu\delta_2}{2}\|\boldsymbol{v}_h^{k}\|_{\Omega_T}^2+\\
&\sum_{k=1}^{j}\tau\delta_1\|\boldsymbol{E}_h^{k+1}-\boldsymbol{E}_h^{k}\|_{\Omega_T}^2+\sum_{k=1}^{j}\frac{\tau\mu}{2\delta_2}\|\boldsymbol{H}_h^{k+1}-\boldsymbol{H}_h^{k}\|_{\Omega_T}^2,
\end{aligned}$$

and together with

$$\mathcal{E}^{j-1}=\frac{\epsilon}{2}\|\boldsymbol{E}_h^{j-1}\|_{\Omega_T}^2+\frac{\mu}{2}\|\boldsymbol{H}_h^{j-1}\|_{\Omega_T}^2+\frac{\tau\omega\mu}{2}\|\boldsymbol{v}_h^{j-1}\|_{\Omega_T}^2+\frac{\mu C_e}{2}\|\nabla\boldsymbol{m}_h^{j-1}\|_{\Omega_T}^2.$$

we obtain that

$$\begin{aligned}\mathcal{E}^{j-1}+\left(\frac{\epsilon}{2}-\tau\delta_1\right)\left(\sum_{k=1}^{i}\|\boldsymbol{E}_h^{k+1}-\boldsymbol{E}_h^{k}\|_{\Omega_T}^2\right)+\tau\sigma\sum_{k=1}^{i}\|\boldsymbol{E}_h^{k}\|_{\Omega_T}^2+\\ \frac{\mu}{2}\left(1-\frac{\tau}{\delta_2}\right)\left(\sum_{k=1}^{i}\|\boldsymbol{H}_h^{k+1}-\boldsymbol{H}_h^{k}\|_{\Omega_T}^2\right)+\\ \tau\mu\left(\alpha-\frac{\delta_2}{2}\right)\sum_{k=1}^{j}\|\boldsymbol{v}_h^{k}\|_{\Omega_T}^2+\frac{\tau\omega\mu}{2}\left(\sum_{k=1}^{j}\|\boldsymbol{v}_h^{k+1}-\boldsymbol{v}_h^{k}\|_{\Omega_T}^2\right)-\\ \mu C_e\tau^2\left(\frac{1}{2}-\theta\right)\sum_{k=1}^{j}\|\nabla\boldsymbol{v}_h^{k}\|_{\Omega_T}^2+\tau\sum_{k=1}^{j}\left\langle\begin{pmatrix}\phi^k\\ \psi^k\end{pmatrix},B\begin{pmatrix}\phi^{k+1}\\ \psi^{k+1}\end{pmatrix}\right\rangle_{\Gamma}\leq\\ \sum_{k=1}^{j}\frac{\tau}{2\delta_1}\|\boldsymbol{J}_h^{k+1}\|_{\Omega_T}^2+\sum_{k=1}^{j}\tau\delta_1\|\boldsymbol{E}_h^{k}\|_{\Omega_T}^2+\mathcal{E}^0\leq\\ \sum_{k=1}^{j}\frac{\tau}{2\delta_1}\|\boldsymbol{J}_h^{k+1}\|_{\Omega_T}^2+\frac{\tau}{2\delta_1}\sum_{k=1}^{j}\mathcal{E}^{k-2}+\mathcal{E}^0.\end{aligned}\tag{4.6}$$

We choose $\delta_1,\delta_2>0$ such that sufficiently small $\tau>0$ satisfy

$$\left(1-\frac{\tau}{\delta_2}\right)>0,\quad \left(\frac{\epsilon}{2}-\tau\delta_1\right)>0\quad\text{and}\quad\left(\alpha-\frac{\delta_2}{2}\right)>0.$$

Estimate equation (4.5) can be simplified to $\mathcal{E}^{j-1}\leq C+c\tau\sum_{i=1}^{j}\mathcal{E}^{j-2}$ and conclude the proof. □

4.3. Existence of weak solution

The next lemma using the Banach-Alaoglu Theorem and Cauchy-Schwarz inequality [14, 24] provides limits of weak solutions.

Lemma 4.3. *There exist functions* $(\boldsymbol{m},\boldsymbol{H},\boldsymbol{E},\tilde{\phi},\tilde{\psi})\in\mathbb{H}^1(\Omega_T,\mathcal{S}^2)\times\mathbb{L}^2(\Omega_T)\times\mathbb{L}^2(\Omega_T)\times\mathbb{L}^2(\mathcal{H}_\Gamma)\times\mathbb{L}^2(\mathcal{H}_\Gamma)$ *such that*

$$\begin{aligned}\boldsymbol{m}_{h,\tau}&\rightharpoonup\boldsymbol{m}\quad\text{in}\quad\mathbb{H}^1(\Omega_T),\\ \boldsymbol{m}_{h,\tau},\boldsymbol{m}_{h,\tau}^{\pm}&\rightharpoonup\boldsymbol{m}\quad\text{in}\quad\mathbb{L}^2([0,T],\mathbb{H}^1(\Omega_T)),\\ \boldsymbol{m}_{h,\tau},\boldsymbol{m}_{h,\tau}^{\pm}&\rightharpoonup\boldsymbol{m}\quad\text{in}\quad\mathbb{L}^2(\Omega_T),\\ \boldsymbol{v}_{h,\tau}^{\pm}&\rightharpoonup\partial_t\boldsymbol{m}\quad\text{in}\quad\mathbb{L}^2(\Omega_T),\\ \boldsymbol{H}_{h,\tau},\boldsymbol{H}_{h,\tau}^{\pm}&\rightharpoonup\boldsymbol{H}\quad\text{in}\quad\mathbb{L}^2([0,T],\mathbb{H}^1(\Omega_T)),\\ \nabla\times\boldsymbol{H}_{h,\tau},\nabla\times\boldsymbol{H}_{h,\tau}^{\pm}&\rightharpoonup\nabla\times\boldsymbol{H}\quad\text{in}\quad\mathbb{L}^2(\Omega_T),\\ \boldsymbol{E}_{h,\tau},\boldsymbol{E}_{h,\tau}^{\pm}&\rightharpoonup\boldsymbol{E}\quad\text{in}\quad\mathbb{L}^2([0,T],\mathbb{H}^1(\Omega_T)),\\ \nabla\times\boldsymbol{E}_{h,\tau},\nabla\times\boldsymbol{E}_{h,\tau}^{\pm}&\rightharpoonup\nabla\times\boldsymbol{E}\quad\text{in}\quad\mathbb{L}^2(\Omega_T),\\ \boldsymbol{\phi}_{h,\tau},\boldsymbol{\phi}_{h,\tau}^{\pm}&\rightharpoonup\tilde{\boldsymbol{\phi}}\quad\text{in}\quad\mathbb{L}^2(\mathcal{H}_\Gamma)\quad\text{w.r.t.}\quad\langle\cdot,\cdot\rangle,\\ \boldsymbol{\psi}_{h,\tau},\boldsymbol{\psi}_{h,\tau}^{\pm}&\rightharpoonup\tilde{\boldsymbol{\psi}}\quad\text{in}\quad\mathbb{L}^2(\mathcal{H}_\Gamma),\quad\text{w.r.t.}\quad\langle\cdot,\cdot\rangle.\end{aligned}$$

We are now able to prove the main result of this paper.

Proof. of theroem 4.1. We proceed for the ILLG (3.1) and Maxwell (3.2) motivated by [9] and [14] respectively.

For any $\varphi \in \mathcal{C}^\infty(\Omega_T)$, $\eta_E, \eta_H \in \mathcal{C}^\infty(\Gamma)$, and $t \in [t_j, t_{j+1})$, we define $\zeta_{h,\tau} = \boldsymbol{m}^-_{h,\tau} \times \varphi$ and $(\eta_{Eh}, \eta_{Hh}) = (\eta_E, \eta_H)$

In equation (3.1) and (3.2), using Definition 3.1 and replacing ζ_h and (η_{Eh}, η_{Hh}) by $\zeta_{h,\tau}(t)$ and $(\eta_{Eh}(t), \eta_{Hh}(t))$ respectively. Then, integrating both sides with respect to t over an interval $[t_j, t_{j+1})$ and summing over j from 0 to $N-1$, we rewrite (3.1) and (3.2) as

$$\begin{aligned} \langle \alpha \boldsymbol{v}^-_{h,\tau}(t), \zeta_{h,\tau}(t)\rangle_{\Omega_T} + \langle \boldsymbol{v}^-_{h,\tau}(t) \times \boldsymbol{m}^-_{h,\tau}(t), \zeta_{h,\tau}(t)\rangle_{\Omega_T} + \\ \langle \omega(\boldsymbol{v}_{h,\tau}(t) - \boldsymbol{v}^-_{h,\tau}(t))/\tau, \zeta_{h,\tau}(t)\rangle_{\Omega_T} + \\ \langle C_e \nabla(\boldsymbol{m}^-_{h,\tau}(t) + \theta\tau \boldsymbol{v}^-_{h,\tau}(t)), \nabla\zeta_{h,\tau}(t)\rangle_{\Omega_T} - \langle \boldsymbol{H}^-_{h,\tau}(t), \zeta_{h,\tau}(t)\rangle_{\Omega_T} = 0, \end{aligned} \tag{4.7}$$

$$\begin{aligned} \langle (\epsilon/\tau + \sigma)\, \boldsymbol{E}_{h,\tau}(t), \eta_{Eh}(t)\rangle_{\Omega_T} - \langle \nabla \times \boldsymbol{H}_{h,\tau}(t), \eta_{Eh}(t)\rangle_{\Omega_T} = \\ \langle (\epsilon/\tau)\boldsymbol{E}^-_{h,\tau}(t), \eta_{Eh}(t)\rangle_{\Omega_T} - \langle \boldsymbol{J}_{h,\tau}(t), \eta_{Eh}(t)\rangle_{\Omega_T}, \\ \langle (\mu/\tau)\boldsymbol{H}_{h,\tau}(t), \eta_{Hh}(t)\rangle_{\Omega_T} + \langle \nabla \times \boldsymbol{E}_{h,\tau}(t), \eta_{Hh}(t)\rangle_{\Omega_T} = \\ \langle (\mu/\tau)\boldsymbol{H}^-_{h,\tau}(t), \eta_{Hh}(t)\rangle_{\Omega_T} - \langle \mu \boldsymbol{v}^-_{h,\tau}(t), \eta_{Hh}(t)\rangle_{\Omega_T}, \\ \left\langle \begin{pmatrix} u^{h,\tau}_\phi(t) \\ u^{h,\tau}_\psi(t) \end{pmatrix}, B \begin{pmatrix} \phi_{h,\tau}(t) \\ \psi_{h,\tau}(t) \end{pmatrix} \right\rangle_\Gamma = \frac{1}{2} \left\langle \begin{pmatrix} u^{h,\tau}_\phi(t) \\ u^{h,\tau}_\psi(t) \end{pmatrix}, \begin{pmatrix} \mu_0^{-1}\gamma_L \boldsymbol{E}_{h,\tau}(t) \\ -\gamma_L \boldsymbol{H}_{h,\tau}(t) \end{pmatrix} \right\rangle_\Gamma. \end{aligned} \tag{4.8}$$

The nodal interpolation operator properties with $\zeta_{h,\tau} = \boldsymbol{m}^-_{h,\tau} \times \varphi$ and $(\eta_{Eh}(t), \eta_{Hh}(t)) = (\eta_{Eh}, \eta_{Hh})$ give

$$\begin{aligned} \langle \alpha \boldsymbol{v}^-_{h,\tau}, \boldsymbol{m}^-_{h,\tau} \times \varphi\rangle_{\Omega_T} + \langle \boldsymbol{v}^-_{h,\tau} \times \boldsymbol{m}^-_{h,\tau}, \boldsymbol{m}^-_{h,\tau} \times \varphi\rangle_{\Omega_T} + \\ \langle \omega(\boldsymbol{v}_{h,\tau} - \boldsymbol{v}^-_{h,\tau})/\tau, \boldsymbol{m}^-_{h,\tau} \times \varphi\rangle_{\Omega_T} + \\ \langle C_e \nabla(\boldsymbol{m}^-_{h,\tau} + \theta\tau \boldsymbol{v}^-_{h,\tau}), \nabla(\boldsymbol{m}^-_{h,\tau} \times \varphi)\rangle_{\Omega_T} - \langle \boldsymbol{H}^-_{h,\tau}, \boldsymbol{m}^-_{h,\tau} \times \varphi\rangle_{\Omega_T} = O(h), \end{aligned} \tag{4.9}$$

$$\begin{aligned} \langle (\epsilon/\tau + \sigma)\, \boldsymbol{E}_{h,\tau}, \eta_{Eh}\rangle_{\Omega_T} - \langle \nabla \times \boldsymbol{H}_{h,\tau}, \eta_{Eh}\rangle_{\Omega_T} = \\ \langle (\epsilon/\tau)\boldsymbol{E}^-_{h,\tau}, \eta_{Eh}\rangle_{\Omega_T} - \langle \boldsymbol{J}_{h,\tau}, \eta_{Eh}\rangle_{\Omega_T}, \\ \langle (\mu/\tau)\boldsymbol{H}_{h,\tau}, \eta_{Hh}\rangle_{\Omega_T} + \langle \nabla \times \boldsymbol{E}_{h,\tau}, \eta_{Hh}\rangle_{\Omega_T} = \\ \langle (\mu/\tau)\boldsymbol{H}^-_{h,\tau}, \eta_{Hh}\rangle_{\Omega_T} - \langle \mu \boldsymbol{v}^-_{h,\tau}, \eta_{Hh}\rangle_{\Omega_T}, \\ \left\langle \begin{pmatrix} u^{h,\tau}_\phi \\ u^{h,\tau}_\psi \end{pmatrix}, B \begin{pmatrix} \phi_{h,\tau} \\ \psi_{h,\tau} \end{pmatrix} \right\rangle_\Gamma = \frac{1}{2} \left\langle \begin{pmatrix} u^{h,\tau}_\phi \\ u^{h,\tau}_\psi \end{pmatrix}, \begin{pmatrix} \mu_0^{-1}\gamma_L \boldsymbol{E}_{h,\tau} \\ -\gamma_L \boldsymbol{H}_{h,\tau} \end{pmatrix} \right\rangle_\Gamma. \end{aligned} \tag{4.10}$$

In order to show that a weak solution $\boldsymbol{m}, \boldsymbol{E}, \boldsymbol{H}, \phi, \psi$ satisfy Definition 2.1, we prove that as h and τ tend to 0.

First, using the strong $\mathbb{L}^2(\Omega_T)$-convergence of $\boldsymbol{m}^-_{h,\tau} \times \varphi$ towards $\boldsymbol{m} \times \varphi$ and bound-

edness of $\tau\|\nabla \boldsymbol{v}^-_{h,\tau}\|^2_{\mathbb{L}^2(\Omega_T)}$ for $\theta \in (1/2, 1]$ from ILLG equation (4.9) we obtain

$$\begin{aligned}
\langle \alpha \boldsymbol{v}^-_{h,\tau} + \boldsymbol{v}^-_{h,\tau} \times \boldsymbol{m}^-_{h,\tau}, \boldsymbol{m}^-_{h,\tau} \times \varphi\rangle_{\Omega_T} &\to \langle \alpha \partial_t \boldsymbol{m} + \partial_t \boldsymbol{m} \times \boldsymbol{m}, \boldsymbol{m} \times \varphi\rangle_{\Omega_T},\\
\langle \omega(\boldsymbol{v}_{h,\tau} - \boldsymbol{v}^-_{h,\tau})/\tau, \boldsymbol{m}^-_{h,\tau} \times \varphi\rangle_{\Omega_T} &\to \langle \omega \partial_{tt} \boldsymbol{m}, \boldsymbol{m} \times \varphi\rangle_{\Omega_T},\\
\langle C_e \nabla \boldsymbol{m}^-_{h,\tau}, \nabla(\boldsymbol{m}^-_{h,\tau} \times \varphi)\rangle_{\Omega_T} &\to \langle C_e \nabla \boldsymbol{m}, \nabla(\boldsymbol{m} \times \varphi)\rangle_{\Omega_T}, \qquad (4.11)\\
\langle \theta\tau \nabla \boldsymbol{v}^-_{h,\tau}, \nabla(\boldsymbol{m}^-_{h,\tau} \times \varphi)\rangle_{\Omega_T} &\to 0 \quad \text{and}\\
\langle \boldsymbol{H}^-_{h,\tau}, \boldsymbol{m}^-_{h,\tau} \times \varphi\rangle_{\Omega_T} &\to \langle \boldsymbol{H}, \boldsymbol{m} \times \varphi\rangle_{\Omega_T}.
\end{aligned}$$

We have now proved

$$\begin{aligned}
\langle \alpha \partial_t \boldsymbol{m} + \partial_t \boldsymbol{m} \times \boldsymbol{m}, \boldsymbol{m} \times \varphi\rangle_{\Omega_T} + \langle \omega \partial_{tt} \boldsymbol{m}, \boldsymbol{m} \times \varphi\rangle_{\Omega_T} =\\
-\langle C_e \nabla \boldsymbol{m}, \nabla(\boldsymbol{m} \times \varphi)\rangle_{\Omega_T} + \langle \boldsymbol{H}, \boldsymbol{m} \times \varphi\rangle_{\Omega_T}.
\end{aligned}$$

The equality $\boldsymbol{m}(0) = \boldsymbol{m}^0$ in the trace sense follows from the weak convergence $\boldsymbol{m}_{h,\tau} \rightharpoonup \boldsymbol{m} \in \mathbb{H}^1(\Omega_T)$ and thus weak convergence of the traces. We eventually determined the limit using the weak convergence $\boldsymbol{m}^0_h \rightharpoonup \boldsymbol{m}^0 \in \mathbb{L}^2(\Omega)$.
Second using Definition 3.1 from Maxwell equation (4.10) we obtain

$$\begin{aligned}
\langle (\epsilon/\tau + \sigma)\, \boldsymbol{E}_{h,\tau}, \eta_{Eh}\rangle_{\Omega_T} &\to \langle (\epsilon/\tau + \sigma)\, \boldsymbol{E}, \eta_E\rangle_{\Omega_T},\\
\langle \nabla \times \boldsymbol{H}_{h,\tau}, \eta_{Eh}\rangle_{\Omega_T} &\to \langle \nabla \times \boldsymbol{H}, \eta_E\rangle_{\Omega_T},\\
\langle (\epsilon/\tau) \boldsymbol{E}^-_{h,\tau}, \eta_{Eh}\rangle_{\Omega_T} &\to \langle (\epsilon/\tau) \boldsymbol{E}, \eta_E\rangle_{\Omega_T},\\
\langle \boldsymbol{J}_{h,\tau}, \eta_{Eh}\rangle_{\Omega_T} &\to \langle \boldsymbol{J}, \eta_E\rangle_{\Omega_T},\\
\langle (\mu/\tau) \boldsymbol{H}_{h,\tau}, \eta_{Hh}\rangle_{\Omega_T} &\to \langle (\mu/\tau) \boldsymbol{H}, \eta_H\rangle_{\Omega_T},\\
\langle \nabla \times \boldsymbol{E}_{h,\tau}, \eta_{Hh}\rangle_{\Omega_T} &\to \langle \nabla \times \boldsymbol{E}, \eta_H\rangle_{\Omega_T},\\
\langle (\mu/\tau) \boldsymbol{H}^-_{h,\tau}, \eta_{Hh}\rangle_{\Omega_T} &\to \langle (\mu/\tau) \boldsymbol{H}, \eta_H\rangle_{\Omega_T},\\
\langle \mu \boldsymbol{v}^-_{h,\tau}, \eta_{Hh}\rangle_{\Omega_T} &\to \langle \mu \partial_t \boldsymbol{m}, \eta_H\rangle_{\Omega_T},\\
\left\langle \begin{pmatrix} u^{h,\tau}_\phi \\ u^{h,\tau}_\psi \end{pmatrix}, B \begin{pmatrix} \phi_{h,\tau} \\ \psi_{h,\tau} \end{pmatrix} \right\rangle_\Gamma &\to \left\langle \begin{pmatrix} u_\phi \\ u_\psi \end{pmatrix}, B \begin{pmatrix} \phi \\ \psi \end{pmatrix} \right\rangle_\Gamma,\\
\frac{1}{2}\left\langle \begin{pmatrix} u^{h,\tau}_\phi \\ u^{h,\tau}_\psi \end{pmatrix}, \begin{pmatrix} \mu_0^{-1}\gamma_L \boldsymbol{E}_{h,\tau} \\ -\gamma_L \boldsymbol{H}_{h,\tau} \end{pmatrix} \right\rangle_\Gamma &\to \frac{1}{2}\left\langle \begin{pmatrix} u_\phi \\ u_\psi \end{pmatrix}, \begin{pmatrix} \mu_0^{-1}\gamma_L \boldsymbol{E} \\ -\gamma_L \boldsymbol{H} \end{pmatrix} \right\rangle_\Gamma.
\end{aligned}$$

Using triangular and Holders inequalities, we show the energy estimate

$$\begin{aligned}
\|\nabla \boldsymbol{m}\|^2_{\mathbb{L}^2(\Omega_T)} + \|\partial_t \boldsymbol{m}\|^2_{\mathbb{L}^2(\Omega_T)} + \|\partial_{tt} \boldsymbol{m}\|^2_{\mathbb{L}^2(\Omega_T)} + \|\boldsymbol{H}\|^2_{\mathbb{L}^2(\Omega_T)} + \|\boldsymbol{E}\|^2_{\mathbb{L}^2(\Omega_T)} \le\\
C\|\nabla \boldsymbol{m}^-_{h,\tau}\|^2_{\mathbb{L}^2(\Omega_T)} + \|\partial_t \boldsymbol{m}_{h,\tau}\|^2_{\mathbb{L}^2(\Omega_T)} + \|\partial_{tt} \boldsymbol{m}_{h,\tau}\|^2_{\mathbb{L}^2(\Omega_T)} +\\
\|\boldsymbol{H}_{h,\tau}\|^2_{\mathbb{L}^2(\Omega_T)} + \|\boldsymbol{E}_{h,\tau}\|^2_{\mathbb{L}^2(\Omega_T)}.
\end{aligned}$$

where we have assumed convergence of initial data satisfies Definition 2.1. The desired result follows from the conservation of energy argument [20]. Thus, we conclude the proof. □

5. Computational experiments and conclusion

In this section, we implement Algorithm 1 in the finite element software *FENICS* [22] and the boundary element software *bempp* [23] on a desktop computer. We

observed that the cost per time step is approximately proportional to the number of mesh elements, although further research beyond the scope of this study is required to establish this conclusion. After discretization, we write MILLG equations (3.1) and (3.2) in the following bilinear form and blocked formulation.

5.1. FEM Implementation

We write this as the following bilinear equation using the saddle point approach [14, 19] for simplicity and solve for $(\boldsymbol{v}_h^j, \lambda_h)$ such that for all (ζ_h, β_h)

$$\begin{aligned}\langle \alpha \boldsymbol{v}_h^j, \zeta_h\rangle_{\Omega_T} - \langle (\boldsymbol{m}_h^j \cdot \boldsymbol{v}_h^j), \beta_h\rangle_{\Omega_T} - \langle (\boldsymbol{m}_h^j \cdot \zeta_h), \lambda_h\rangle_{\Omega_T} + \langle \boldsymbol{v}_h^j \times \boldsymbol{m}_h^j, \zeta_h\rangle_{\Omega_T} + \\ \langle \omega(\boldsymbol{v}_h^{j+1} - \boldsymbol{v}_h^j)/\tau, \zeta_h\rangle_{\Omega_T} = -\langle \nabla \boldsymbol{m}_h^{j+1}, \nabla \zeta_h\rangle_{\Omega_T} + \langle \boldsymbol{H}_h^j, \zeta_h\rangle_{\Omega_T},\end{aligned}$$

$$LHS^{j+1} = RHS^j.$$

The terms orthogonal to the test functions may be theoretically dropped but are relevant for saddle point approach conditioning.

5.2. BEM Implementation

Discrete spaces from natural standard grids, barrycentrically refined grids, and edge-scaled grids mostly naturally generate the same and mathematically identical basis functions. However, for implementation, inner products can only be computed by basis functions defined on the same grid.
Let $\boldsymbol{F}$ be a Linear operator in *bempp*. Then $\boldsymbol{F}$ is the matrix that maps coefficients of functions $\boldsymbol{P}$ in Domain Space, DS, to coefficients of $\boldsymbol{P}$ in Range Space, RS, tested with functions in the Dual Space to Range Space, $DSRS$.
We can denote ${}^{DSRS}\boldsymbol{F}^{DS}$ as a weak form of $\boldsymbol{F}$ and $\boldsymbol{F}^{DS\to RS}$ as a strong form of $\boldsymbol{F}$ which are related as follows

$${}^{DSRS}\boldsymbol{F}^{DS} = ({}^{DSRS}\boldsymbol{Id}^{DS})\boldsymbol{F}^{DS\to RS}.$$

The strong form can be expressed as

$$(FP)(RS) = \boldsymbol{F}^{DS\to RS} \cdot \boldsymbol{P}(DS).$$

Using the standard basis functions from discrete element spaces such as Scalar Linear, $S1$, Vector-Valued, $S1$, First Order Nedelec, $N1$, Raviart Thomas, RT and Nedelec, NC. Scaled basis functions such as Rao-Wilton-Glisson, RWG, and Scaled Nedelec, SNC spaces are also used. There are also barrycentrical basis functions, to mention but a few Buffa-Christiansen, BC, and Rotated Buffa-Christiansen, RBC. The basis function can be defined by rotation and scaling of the corresponding basis function. The change of basis function can be implemented via the application of $\boldsymbol{n}\times(\cdots)$ or multiplication by the associated edge to obtain an identical basis function. Summarize and state the full system by defining mass matrices

$$\boldsymbol{Q}_0 := ({}^{N1}\boldsymbol{Id}^{N1}),$$

$$\boldsymbol{Q}_1 := ({}^{N1}\boldsymbol{Id}^{S1}),$$

$$\boldsymbol{Q}_2 := ({}^{NC}\boldsymbol{Id}^{NC}),$$

$$\boldsymbol{Q}_3 := ({}^{RBC}\boldsymbol{Id}^{RWG})\boldsymbol{\gamma_T}^{N1\to RT},$$

$$\boldsymbol{Q}_4 := ({}^{RBC}\boldsymbol{Id}^{RWG})\boldsymbol{\gamma_T}^{RBC\to RWG},$$

$$\boldsymbol{Q}_5 := ({}^{RBC}\hat{\boldsymbol{E}}^{RWG}).$$

Define the symmetric, discrete differential operator

$$D := 0.5({}^{NC}\boldsymbol{\nabla}\times{}^{NC}) + 0.5({}^{NC}\boldsymbol{\nabla}\times{}^{NC})^T.$$

Full Blocked formulation

$$\begin{bmatrix} \left(\frac{\epsilon}{\tau}+\sigma\right)\boldsymbol{Q}_2\boldsymbol{E}^{i+1} & -D\boldsymbol{H}^{i+1} & -\mu_0^{-1}\boldsymbol{Q}_3^T\boldsymbol{E}^{i+1} & 0 \\ D\boldsymbol{E}^{i+1} & \frac{\mu_0}{\tau}\boldsymbol{Q}_2\boldsymbol{H}^{i+1} & 0 & -\boldsymbol{Q}_3^T\boldsymbol{H}^{i+1} \\ \mu_0^{-1}\boldsymbol{Q}_3\boldsymbol{E}^{i+1} & 0 & -\mu_0^2\sqrt{\mu_0\epsilon}\boldsymbol{Q}_5 & \mu_0^{-1}\boldsymbol{Q}_5 \\ 0 & \boldsymbol{Q}_3\boldsymbol{H}^{i+1} & -\mu_0\boldsymbol{Q}_5 & \sqrt{\mu_0\epsilon}\boldsymbol{Q}_5 \end{bmatrix} \begin{bmatrix} \boldsymbol{E}^{i+1} \\ \boldsymbol{H}^{i+1} \\ \boldsymbol{\phi}^{i+1} \\ \boldsymbol{\psi}^{i+1} \end{bmatrix} =$$

$$\begin{bmatrix} Y[0] \\ Y[1] \\ Y[2] \\ Y[3] \end{bmatrix} = \begin{bmatrix} \frac{\epsilon}{\tau}\boldsymbol{Q}_0\boldsymbol{E}^i - \boldsymbol{Q}_1\boldsymbol{J}^{i+1} \\ \frac{\mu_0}{\tau}\boldsymbol{Q}_0\boldsymbol{H}^i - \boldsymbol{Q}_1\boldsymbol{v}^i \\ -\boldsymbol{Q}_4\boldsymbol{E}^i - \boldsymbol{E}_{inc} \\ \mu_0\boldsymbol{Q}_4\boldsymbol{H}^i - \boldsymbol{H}_{inc} \end{bmatrix},$$

$$LHS \begin{bmatrix} \boldsymbol{E}^{i+1}(\chi_h) \\ \boldsymbol{H}^{i+1}(\chi_h) \\ \boldsymbol{\phi}^{i+1}(RBC) \\ \boldsymbol{\psi}^{i+1}(RWG) \end{bmatrix} = RHS^i.$$

5.3. Convergence in time and space

In this research, consider convergence with rates of the Maxwell-Inertia-Landau-Lifshitz-Gilbert (MILLG) system. We implement an algorithm for the approximation of the MILLG system that, provided the exact solution is smooth enough, converges to the solution with a priori-know error ratio. Two academic examples are performed to solve the problem of an effective magnetic field on a unit cube, $\Omega_1 = (0,1)^3$ and thin plate $\Omega_2 = (0,1)\times(0,1)\times(0,0.08)$ of ferromagnetic material with different material parameters inside and outside the domain.

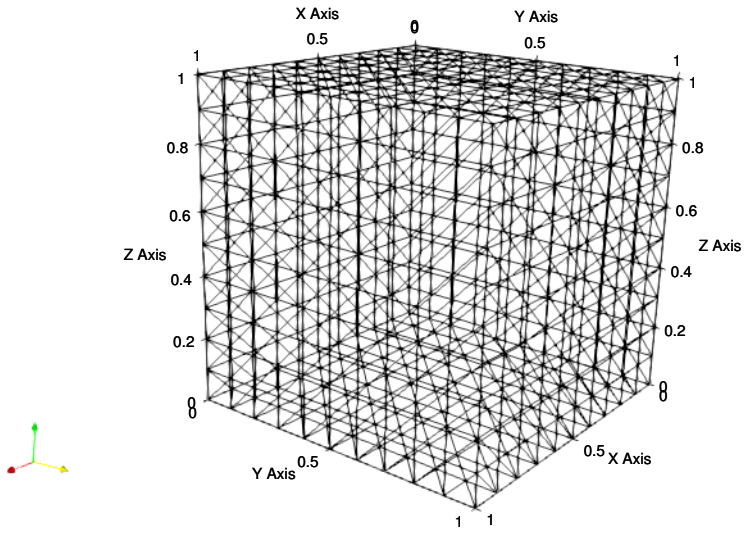

Figure 1. The representation of cube tetrahedral mesh with a total of 3996 nodes in the domain (left) and cube surface with edges representation (right)

The tolerance for the iterative solver (GMRES) is set to 10^{-8}, the implicity parameter for the tangent plane scheme $\theta = 1$. We investigate the spatial discretization error on a fixed time grid. The following prescribed exact solution from previous work [9, 14] has been used

$$\begin{aligned} \boldsymbol{m}(x,t) &:= \begin{bmatrix} -(x_1^3 - \frac{3}{2}x_1^2 + \frac{1}{4})\sin\frac{3\pi t}{10T} \\ \sqrt{1-(x_1^3 - \frac{3}{2}x_1^2 + \frac{1}{4})} \\ -(x_1^3 - \frac{3}{2}x_1^2 + \frac{1}{4})\cos\frac{3\pi t}{10T} \end{bmatrix}, \\ \boldsymbol{E}(t,x) &= t^2\left[\sin(\pi x_1)^2\sin(\pi x_2)^2\sin(\pi x_3)^2, 0, 0\right], \\ \boldsymbol{H} = -\partial_t^{-1}\nabla\times\boldsymbol{E} &= 4t\begin{bmatrix} 0 \\ \sin(\pi x_1)\cos(\pi x_1)\sin(\pi x_2)^2\sin(\pi x_3)^2 \\ \sin(\pi x_1)^2\sin(\pi x_2)\cos(\pi x_2)\sin(\pi x_3)^2 \end{bmatrix}, \\ \phi &= \psi = 0. \end{aligned} \tag{5.1}$$

The electric field $\boldsymbol{E}$ is the sum of the incident field $\boldsymbol{E}_{\text{inc}}$ and the scattered field $\boldsymbol{E}^{\text{s}}$. Here, we use the incident field given by

$$\boldsymbol{E}_{\text{inc}}(\boldsymbol{x}) := \left[\exp(\mathrm{i}kd)\ 0\ 0\right],$$

where k denotes the wave number which is traveling in the d direction and polarized in the $\boldsymbol{x}$ direction.

We choose the material parameters as $T = 0.125$, $\epsilon_0 = \epsilon = 1.1$, $\mu_0 = \mu = 1.2$, $\sigma = 1.3$, $\alpha = 1.4$, $C_e = 1.5$. We used the initial and input data as $\boldsymbol{m}^0 =$

$[\sin(\pi x_1)\cos(\pi x_2)\cos(\pi x_3), -\cos(\pi x_1)\sin(\pi x_2)\cos(\pi x_3), \cos(\pi/12)]$, $\boldsymbol{E}^0 = \boldsymbol{H}^0 = [0,0,0]$, $\phi^0 = \psi^0 = [0,0,0]$, $\boldsymbol{J} = [100,0,0]$.
Compute the time discretization errors with corresponding $\mathbb{L}^2$-projections of the discretized data on a unit cube Ω_1 fixed coarse mesh. For time step sizes $\tau_i = T \cdot 2^{-j}, j = 0, ..., 8$, the computed approximations are compared with the reference solution computed on a fine time grid $\tau_{\text{ref}} = 2^{-9}$ and obtain their first-order convergence from respective norms as:

$$err_{R,j} = \max_{j=0,\ldots,N} \|R_h^j - R_h^{\text{ref}}(t_j)\|, \quad \boldsymbol{R} \in \{\boldsymbol{m}, \boldsymbol{E}, \boldsymbol{H}, \phi, \psi\}.$$

For a fixed time grid and a shorter time horizon $T = 0.125$, and a varied coarse mesh on a thin plate Ω_2. Compute the spatial discretization errors by comparing the computed approximations with the given exact solution. By using the exact solution 5.1, one can ignore the error induced by time discretization, and we obtain first-order convergence from their respective norms as:

$$err_{R,j} = \max_{j=0,\ldots,N} \|R_{h_k}^j - R(t_j)\|, \quad \boldsymbol{R} \in \{\boldsymbol{m}, \boldsymbol{E}, \boldsymbol{H}, \phi, \psi\}.$$

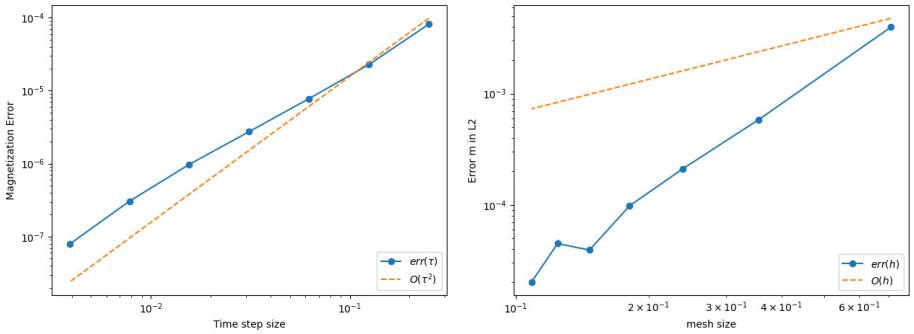

(a) $\boldsymbol{m}$ solution versus the time step size (b) $\boldsymbol{m}$ solution versus the mesh size

Figure 2. Experimental error of magnetization $\boldsymbol{m}$ solution versus the time step size and mesh size

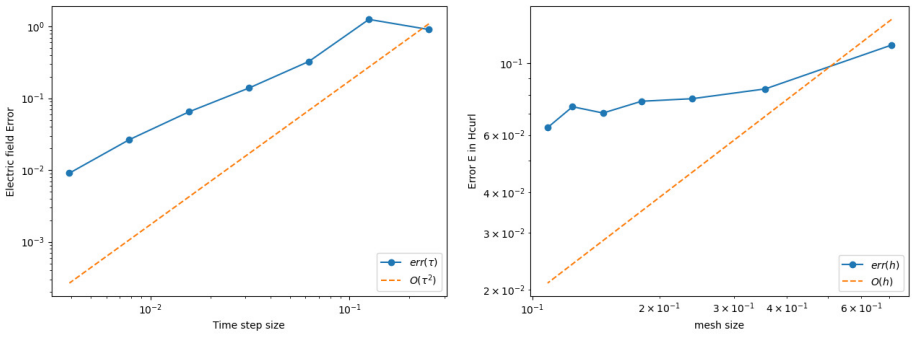

(a) $\boldsymbol{E}$ solution versus the time step size (b) $\boldsymbol{E}$ solution versus the mesh size

Figure 3. Experimental error of electric field $\boldsymbol{E}$ solution versus the time step size and mesh size

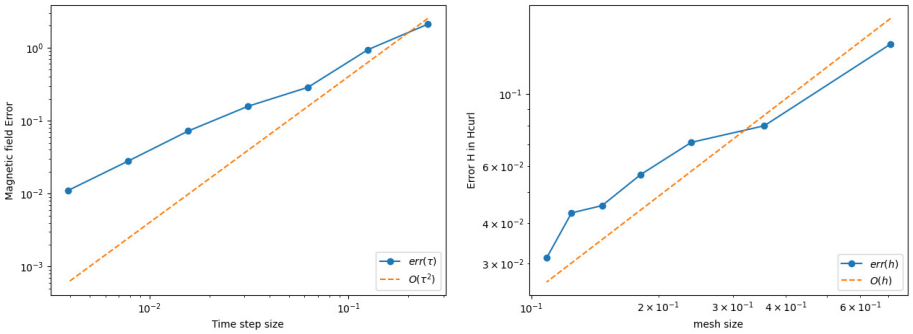

(a) $\boldsymbol{H}$ solution versus the time step size (b) $\boldsymbol{H}$ solution versus the mesh size

Figure 4. Experimental error of magnetic field $\boldsymbol{H}$ solution versus the time step size and mesh size

Figures (2, 3 and 4) show the error in magnetization, electric field, and magnetic field solutions, respectively. The error measured in the $\mathbb{L}^2$ norm changes as the time step size used in the simulation varies. The error generally decreases as the time step size is reduced. Figures (5, 6 and 7) show the error in magnetization, electric field, and magnetic field solutions, respectively. The error measured in the $\mathbb{L}^2$ norm changes as the mesh size used in the simulation varies. The error generally decreases as the mesh size is reduced. The dashed line labeled $O(\tau^2)$ indicates an approximate second-order convergence rate. The observed second-order convergence suggests that the numerical method used in the simulation is reasonably accurate.

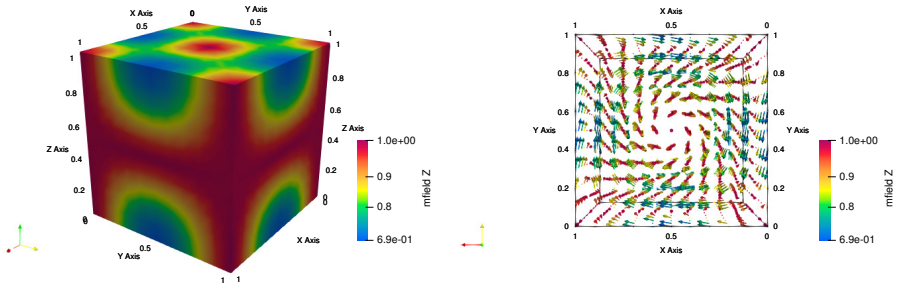

(a) $\boldsymbol{m}$ surface view (b) $\boldsymbol{m}$ glyph view

Figure 5. The vectors in the plots denote the magnetization solution components, and the color denotes the $\boldsymbol{m}_z$ component in z-direction

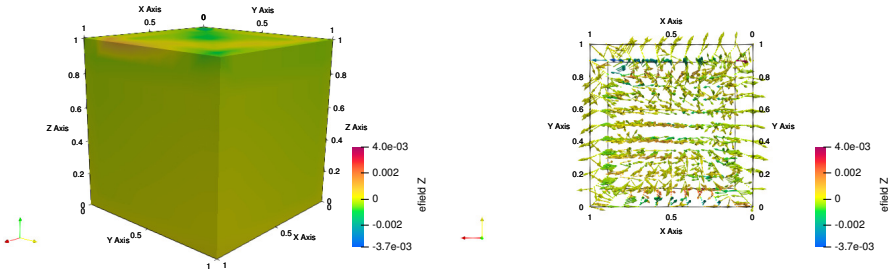

(a) $\boldsymbol{E}$ surface view (b) $\boldsymbol{E}$ glyph view

Figure 6. The vectors in the plots denote the electric field solution components, and the color denotes the $\boldsymbol{E}_z$ component in z-direction

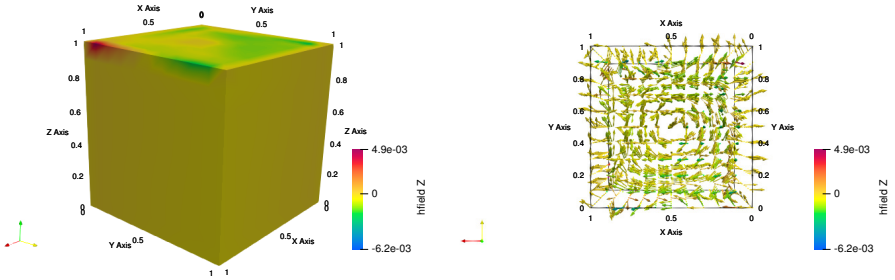

(a) $\boldsymbol{H}$ surface view (b) $\boldsymbol{H}$ glyph view

Figure 7. The vectors in the plots denote the magnetic field solution components, and the color denotes the $\boldsymbol{H}_z$ component in z-direction

Figures (5-7) show magnetization, electric field, and magnetic field inside the domain. The simulation solution of the z component quantities fluctuates as observed with the direction arrows and on the surface.

5.4. Conclusions

We have given FEM-BEM convergence analysis for the coupled MILLG equations. A convergence theorem is also given, improving known results in the literature. We have not included timing benchmarks in this work since the goal is to account for relevant magnetization dynamics contributions and functional analytic approaches and not the performance comparison of different frameworks. The convergence analysis extends directly to ILLG after incorporating inertia effects into LLG. Similarly, for Maxwell, from time-dependent boundary integral to space-dependent formulation. We are aware that optimal order error bounds of LLG has been established theoretically [19]. In the future work, theoretical analysis can be extended to ILLG. For this case, we demonstrated reasonably accurate simulations by utilization of numerical experiments to vary time steps and mesh sizes. In the subsequent work, we will extend the theoretical analysis to establish optimal convergence rate and error estimate under suitable regularity assumptions and the reasonable ratio between

time step size and spatial mesh size [25]. Numerical examples are also provided, showing the practical applicability of the method.

Declaration of competing interest

The authors declare that they have no known competing financial interests or personal relationships that could have appeared to influence the work reported in this paper.

Acknowledgments

This work is partly supported by the National Natural Science Foundation of China [Grant No. 51974377] and the China Scholarship Council [Grant No. 2020GBJ00921].

References

[1] M. Lakshmanan, The fascinating world of the Landau–Lifshitz–Gilbert equation: an overview, Philosophical Transactions of the Royal Society A: Mathematical, Physical and Engineering Sciences 369 (2011) 1280–1300. doi:10.1098/rsta.2010.0319.

[2] M. Feischl, T. Tran, Existence of regular solutions of the Landau–Lifshitz–Gilbert equation in 3d with natural boundary conditions, SIAM Journal on Mathematical Analysis 49 (2017) 4470–4490. doi:10.1137/16M1103427.

[3] P. Zhong, F. Wu, S. Tang, Renormalization for the laplacian and global well-possness of the Landau–Lifshitz–Gilbert equation in dimensions $n \geq 3$, Boundary Value Problems 2020 (2020) 96. doi:10.1186/s13661-020-01377-6.

[4] L. Kim-Ngan, T. Thanh, A convergent finite element approximation for the quasi-static Maxwell–Landau–Lifshitz–Gilbert equations, Computers and Mathematics with Applications 66 (2013) 1389–1402. doi:10.1016/j.camwa.2013.08.009.

[5] Y. Cai, J. Chen, C. Wang, C. Xie, A second-order numerical method for Landau-Lifshitz-Gilbert equation with large damping parameters, Journal of Computational Physics 451 (2022) 110831. doi:10.1016/j.jcp.2021.110831.

[6] J. Chen, C. Wang, C. Xie, Convergence analysis of a second-order semi-implicit projection method for Landau-Lifshitz equation, Applied Numerical Mathematics 168 (2021) 55–74. doi:10.1016/j.apnum.2021.05.027.

[7] E. Kim, K. Lipnikov, The mimetic finite difference method for the Landau–Lifshitz equation, Journal of Computational Physics 328 (2017) 109–130. doi:https://doi.org/10.1016/j.jcp.2016.10.016.

[8] B. Li, J. Wang, L. Xu, A convergent linearized lagrange finite element method for the magneto-hydrodynamic equations in two-dimensional nonsmooth and nonconvex domains, SIAM Journal on Numerical Analysis 58 (2020) 430–459. doi:10.1137/18M1205649.

[9] M. Ruggeri, Numerical analysis of the Landau–Lifshitz–Gilbert equation with inertial effects, ESAIM: Mathematical Modelling and Numerical Analysis 56 (2022) 1199–1222. doi:10.1051/m2an/2022043.

[10] A. François, K. Evaggelos, T. Jean-Christophe, A convergent finite element approximation for Landau–lifschitz–Gilbert equation, Physica B: Condensed Matter 407 (9) (2012) 1345–1349. doi:https://doi.org/10.1016/j.physb.2011.11.031.

[11] K. Neeraj, N. Awari, S. Kovalev, D. Polley, N. Zhou Hagström, S. S. P. K. Arekapudi, A. Semisalova, K. Lenz, B. Green, J.-C. Deinert, I. Ilyakov, M. Chen, M. Bawatna, V. Scalera, M. d'Aquino, C. Serpico, O. Hellwig, J.-E. Wegrowe, M. Gensch, S. Bonetti, Inertial spin dynamics in ferromagnets, Nature Physics 17 (2021) 245–250. doi:https://doi.org/10.1038/s41567-020-01040-y.

[12] M.-C. Ciornei, J. M. Rubí, J.-E. Wegrowe, Magnetization dynamics in the inertial regime: Nutation predicted at short time scales, Phys. Rev. B 83 (2011) 020410. doi:10.1103/PhysRevB.83.020410.

[13] I. Cimrák, Existence, regularity and local uniqueness of the solutions to the Maxwell–Landau–Lifshitz system in three dimensions, Journal of Mathematical Analysis and Applications 329 (2007) 1080–1093. doi:https://doi.org/10.1016/j.jmaa.2006.06.080.

[14] J. Bohn, M. Feischl, B. Kovács, Fem-bem coupling for the Maxwell–Landau–Lifshitz–Gilbert equations via convolution quadrature: Weak form and numerical approximation, Computational Methods in Applied Mathematics 23 (2023) 19–48. doi:10.1515/cmam-2022-0145.

[15] B. Goldys, K.-N. Le, T. Tran, A finite element approximation for the stochastic Landau–Lifshitz–Gilbert equation, Journal of Differential Equations 260 (2) (2016) 937–970. doi:https://doi.org/10.1016/j.jde.2015.09.012.

[16] B. Kovács, C. Lubich, Stable and convergent fully discrete interior–exterior coupling of Maxwell's equations, Numerische Mathematik 137 (91) (2017) 117–137. doi:10.1007/s00211-017-0868-8.

[17] M. W. Scroggs, T. Betcke, E. Burman, W. Śmigaj, E. van't Wout, Software frameworks for integral equations in electromagnetic scattering based on calderón identities, Computers and Mathematics with Applications 74 (11) (2017) 2897–2914. doi:https://doi.org/10.1016/j.camwa.2017.07.049.

[18] D. Colton, R. Kress, Boundary-Value Problems for the Time-Harmonic Maxwell Equations and the Vector Helmholtz Equation, 2013, Ch. Chapter 4, pp. 108–149. doi:10.1137/1.9781611973167.ch4.

[19] G. Akrivis, M. Feischl, B. Kovács, C. Lubich, Higher-order linearly implicit full discretization of the Landau–Lifshitz–Gilbert equation, Mathematics of Computation 90 (329) (2021) 995–1038. doi:10.1090/mcom/3597.

[20] G. D. Fratta, M. Innerberger, D. Praetorius, Weak–strong uniqueness for the Landau–Lifshitz–Gilbert equation in micromagnetics, Nonlinear Analysis: Real World Applications 55 (2020) 103122. doi:10.1016/j.nonrwa.2020.103122.

[21] S. Bartels, Stability and convergence of finite-element approximation schemes for harmonic maps, SIAM Journal on Numerical Analysis 43 (1) (2005) 220–238. doi:10.1137/https://doi.org/10.1137/040606594.

[22] M. S. Alnæs, A. Logg, K. B. Ølgaard, M. E. Rognes, G. N. Wells, Unified form language, ACM Transactions on Mathematical Software 40 (2014) 1–37. doi:10.1145/2566630.

[23] T. Betcke, M. W. Scroggs, Bempp-cl: A fast python based just-in-time compiling boundary element library., Journal of Open Source Software 6 (2021) 2879. doi:10.21105/joss.02879.

[24] K.-N. Le, T. Tran, A convergent finite element approximation for the quasi-static Maxwell–Landau–Lifshitz–Gilbert equations, Computers & Mathematics with Applications 66 (8) (2013) 1389–1402. doi:https://doi.org/10.1016/j.camwa.2013.08.009.

[25] Y. Cai, J. Chen, C. Wang, C. Xie, Error analysis of a linear numerical scheme for the landau–lifshitz equation with large damping parameters, Mathematical Methods in the Applied Sciences 46 (18) (2023) 18952–18974. doi:https://doi.org/10.1002/mma.9601.

[26] X. Changjian, J. G.-C. Carlos, W. Cheng, Z. Zhennan, C. Jingrun, Second-order semi-implicit projection methods for micromagnetics simulations, Journal of Computational Physics 404 (2020) 109104. doi:https://doi.org/10.1016/j.jcp.2019.109104.